Running title: PALEOFLOODS AND FIRES IN THE BEDROCK-CONFINED HUIS RIVER, SOUTH AFRICA

A HOLOCENE "FROZEN ACCIDENT": SEDIMENTS OF EXTREME PALEOFLOODS AND FIRES IN THE BEDROCK-CONFINED UPPER HUIS RIVER, WESTERN CAPE, SOUTH AFRICA

EMESE M. BORDY[1], DEVON A. BOWEN[1], JOHN MOORE[2, †], MARK H. GARNETT[3] and HARILAOS TSIKOS[2]

[1]Department of Geological Sciences, University of Cape Town, South Africa; Emese.Bordy@uct.ac.za

[2]Department of Geology, Rhodes University, Grahamstown, South Africa

[3]NERC Radiocarbon Facility at the Scottish Universities Environmental Research Centre (SUERC), UK

[†] - deceased

KEYWORDS:
paleoflood hydrology, radiocarbon dating, charcoal, sediment gravity flows, massive sedimentation events

ABSTRACT

Wildfires and flooding events are common and are forceful intrinsic controls over landscape evolution, biodiversity, and preserved sediment architecture in dryland environments. Charcoal-bearing Holocene flood sediments of the upper Huis River provide a rare perspective on the powerful and episodic sedimentary processes in a bedrock-confined fluvial setting in the tectonically stable SW Cape Fold Belt in South Africa. The sediments described in this paper are associated with high-magnitude, debris-flow-dominated paleofloods, and their charcoal content is linked to a series of radiocarbon-dated Holocene paleofires that occurred from ~ 2165 ± 37 BP to ~ 653 ± 35 BP. The five sedimentary facies associations are documented as products of: a) noncohesive pseudoplastic debris flows; b) transitional, high-matrix-strength debris flows with heterogeneous fluid content and flow behavior; c) low-cohesion debris flows; d) hyperconcentrated flows; and e) fluvial channel flow in the upper Huis River. The last is interpreted mainly from massive, subrounded to subangular boulder bars, which provide key evidence for the dramatic scouring of the upper Huis valley. The paleofloods, which not only filled the valley with debris-flow sediments up to 12 m thick, but also subsequently flushed it out nearly to the bedrock, had estimated extreme discharges of few thousands of m^3/s. In summary, the upper Huis River sediments are exceptional because they preserve the geological record of reoccurring fires, and at least three extreme paleofloods (i.e., massive sedimentation events) over a period of ~ 1500 years in an area typified by the fire-prone and fire-dependent Fynbos Biome. Furthermore, this study provides insights into what the gaps in the commonly fragmented bedrock-confined alluvial stratigraphic record would be like, should there be “more record than gap”.

INTRODUCTION

Wildfires and flooding events are common in seasonally dry environments and are intrinsic driving forces in the evolution of the biodiversity, geomorphology, and sediment architecture in these regions (Florsheim et al., 1991; Soler and Sala, 1992; Ryan et al., 2011; Belcher et al., 2013). As modern processes, wildfires and floods are relatively well understood, but their combined role in shaping the landscape ecology and contributing to the sedimentary record, particularly in and near bedrock-confined fluvial settings, is poorly known (Baker, 1984; Baker and Kochel, 1988; Jansen and Brierley, 2004). Understanding the spectrum of sedimentation-controlling factors acting over variable times scales in fire- and flood-prone regions, however, is important for paleoecologic and paleoclimatic reconstructions, including but not limited to the evolution of the landscape and habitats as well as for potential flood-hazard considerations.

In southern Africa, the land surface has undergone major uplift events since the Mesozoic break-up of Gondwana (Burke and Gunnell, 2008), and in the Cenozoic, the net creation of continental accommodation space was so low that southern Africa is in a nearly steady geomorphic state (Scharf et al., 2013). This is particularly valid for the vicinity of the study area, the SW Cape Fold Belt (Fig. 1), a rugged, mountainous region in the Fynbos Biome, covered by a botanically diverse, highly endemic, evergreen, fire-prone and fire-dependent shrubland dominated by Asteraceae, Fabaceae, Iridaceae, Aizoaceae, Ericaceae, Proteaceae, etc. (Goldblatt and Manning, 2002). The region has a Cenozoic geomorphological history shaped by powerful intrinsic forces (e.g., strong lithological control) rather than extrinsic controls due to neotectonic uplift or sea-level changes (Seydack et al., 2007; Scharf et al., 2013). In this tectonically ultrastable region, the comparative erosion and sediment supply rates are very low, and the preservation potential of the sediments is limited, and therefore its alluvial stratigraphic record has even “more gap than record" (Ager, 1973; Miall, 2014a).

Against this backdrop, the Holocene sediments, which are preserved up to twelve meters above the present-day waterline of the bedrock-confined upper Huis River in the Western Cape, South Africa (Fig. 1), can be considered “frozen accidents” that provide rare insights into the dynamics of: (a) bedrock-confined fluvial sediments known to have low preservation potential (Jansen and Brierley, 2004), and (b) fire- and flood-prone landscapes that typify parts of southern Africa and the SW Cape Fold Belt (Moll et al., 1980; Stear, 1985; Cowling, 1992; Zawada, 1994; Seydack et al., 2007; Damm and Hagedorn, 2010; Scharf et al., 2013). The main objectives of this contribution are to document the record of the extreme flooding in the upper Huis River over an ~ 1500 year time scale and to examine the processes that operated during the massive sedimentation events, which were related to intense downpours and the penecontemporaneous fires as indicated by the abundant charcoal fragments in nearly all of the sediments in the upper Huis River. In brief, the facies analysis presented here leads to a better understanding of the sedimentary dynamics in bedrock-confined rivers, especially where massive sedimentation events dominated by debris flows may be linked to reoccurring wildfires. Depending on the frequency, size, intensity, and annual timing of the fire season, wildfires have been shown to not only shape the landscape but also to influence plant evolution and diversity, especially since the Cretaceous (Bond and Scott, 2010; Belcher et al., 2013; Muir et al., 2015).

GEOLOGICAL AND ECOLOGICAL BACKGROUND

The study area is a situated in the catchment of the upper Huis River at the northern foothills of the Langeberg Range of the SW Cape Fold Belt, southeast of Barrydale, Western Cape, South Africa (Fig. 1). The upper catchment of the Huis River has an elongate shape and is about 12 km long, varying from about 3.5 to 1.5 km in width from base to top (Fig. 1). Peak catchment elevation is at about 1450 m above sea level, and the base at the exit point to the lower catchment is at 415 m above sea level. The upper part of the Huis River catchment, currently of an ephemeral nature, drains an area of approximately 25 km^2 in size (blue dashed line Fig. 1) that is covered by natural fynbos vegetation (Bradshaw and Cowling, 2014). Here, the river has a bedrock base, cutting through resistant quartzites, shales and phyllites of the Ordovician-to-Silurian Nardouw Subgroup (Table Mountain Group, Cape Supergroup; Fig. 1; CGS, 1997). The lower part of the drainage has a wider open valley, traverses phyllites and sandstones of the Devonian Bokkeveld Group (Fig. 1), and is flanked by agricultural lands (deciduous fruit) and human habitation (village of Barrydale), partly sited on Holocene alluvial valley-fill sediments. The upper catchment exits through a meandering incised bedrock canyon cut through folded quartzites (inset in Fig. 1), approximately where the river crosses the contact between the Nardouw Subgroup and the Bokkeveld Group. The canyon floor varies in width from about 20 m wide at the upstream end to about 40 m wide at the downstream end. The floor of the thalweg is highly irregular due to the thick-bedded (± 1 m) nature of the bedrock quartzites (inset in Fig. 1) that tend to part along bedding planes and orthogonal joints. Prominent potholes are present in places, and a waterfall and plunge pool with a combined throw of at least 5 m is present near the upstream end of the canyon.

In the SW Cape Fold Belt, the Langeberg Range represents a regional east-west-trending antiformal structure that, at present exposure levels, is cored by a thick succession of quartzites of the Peninsula Formation (Table Mountain Group; Fig. 1; CGS, 1997). Due to the north-verging nature of the folding quartzites of the overlying Nardouw Subgroup (Table Mountain Group) and phyllites and sandstones of the Ceres Subgroup (Bokkeveld Group) along the northern flank of the mountain range are vertical to overturned and show intense mesoscale folding and low-grade greenschist-facies metamorphism (Hälbich and Cornell, 1983). For the upper half of its extent, the Huis River follows closely the upper contact of the Cedarberg Formation shales in a narrow east-west-striking valley. The reason that it follows the upper contact and not the lower is due to the overturned nature of the sedimentary rocks. The course of the river in the lower half of the upper catchment has a stepped nature, alternately following strike and then crosscutting orthogonally through the quartzites of the Nardouw Subgroup, resulting in a general flow direction to the northwest (Fig. 1). Over the last two kilometers, the river course contains distinct meanders with wavelengths of approximately 500 m. The meanders mimic the mesoscale west-plunging antiformal and synformal structures in the bedrock quartzites, with an identical wavelength but with a lower amplitude. It is this latter meandering part that contains the Holocene sediments of interest.

During this study, the sediments were examined in the river canyon upstream from and at the confluence between the upper Huis River and a minor tributary (Fig. 1). The study continued to the southeast, approximately 1 km upstream from the confluence, where the river narrows after two meanders (Fig. 1). The SW Cape Fold Belt, with its seasonal, Mediterranean-type climate of dry, warm to hot, windy summers and cool, wet winters, is known to experience intense downpours, generally related to sporadic “cut-off low-pressure” phenomena. These convective summer weather conditions have resulted in torrential rainfall, thunderstorms, flash flooding, and substantial transport and deposition of alluvial sediments in the regional drainages (for data on climate and discharge, see, e.g., Stear, 1985; Zawada, 1994; Damm and Hagedorn, 2010; Bradshaw and Cowling, 2014; Benito et al., 2011; Hahn et al., 2017 and references therein). Furthermore, the region is also remarkable for its unique ecosystem of exceptionally high habitat differentiation and fynbos biodiversity, which is not only prone to fire but also adapted and dependent on spatiotemporally variable fire regimes with widely varying fire frequency, size, seasonality, and intensity (Moll et al., 1980; Cowling, 1992; Bond and Van Wilgen, 1996; Seydack et al., 2007; Allsopp et al., 2014; Kraaij and van Wilgen, 2014). Ignition sources of fynbos fires are both natural (lightning, quartzite rock falls) and anthropogenic. The former occurs under hot, dry, and windy conditions associated with the summer months, and the latter is especially significant since the arrival of pastoralists in southern Africa some 2000 years ago (Schapera, 1930; Hall, 1984; Sealy and Yates, 1994; Henshilwood, 1996; Seydack et al., 2007; Kraaij and van Wilgen, 2014; Sadr, 2015).

METHODOLOGY

Facies Analysis

Holocene sediments in the upper Huis River were observed at naturally occurring outcrops using the well-established facies-analysis method described in Miall (1996). The sedimentary facies (Fig. 2) were identified based on their lithology, composition, grain size, fabric and textural characteristics, syn- and post-sedimentary structures as well as nature of their contacts with the overlying and underlying facies. Based on their co-occurrence, the facies were then combined into facies associations (FAs) (Table 1).

The spatial and temporal relationships among the facies and facies associations (Figs. 3 to 10) as well as the geometry of river valley (e.g., measured cross sections; see Table 2) were recorded through the use of field sketches, photographs, and our own land survey data aided by survey rods, clinorule, theodolite, and a high-precision Garmin GPSMap 60CS. A

Leica EZ4D stereo microscope with 4.4:1 zoom was used to evaluate sediment composition and relative grain size of the sediment samples.

Radiocarbon Dating

Selected detrital charcoal and wood samples were collected from *in situ* deposits in the field (Table 1). Samples were prepared to graphite at the Natural Environment Research Council (NERC) Radiocarbon Facility (Environment) and passed to the Scottish Universities Environmental Research Centre (SUERC) Accelerator Mass Spectrometry Facility for ^{14}C analysis. Each sample was initially digested in 2M HCl at 80°C for 8 hours, rinsed of mineral acid residue with deionized water, and then digested in 1M KOH at 80°C for 2 hours. Digestion was repeated using deionized water until no further humics were extracted. The residue was then rinsed free of alkali, digested in 1M HCl at 80°C for 2 hours, rinsed free of acid, dried, and homogenized. The total carbon in a known weight of the pre-treated sample was recovered as CO_2 following combustion in an elemental analyzer. The gas was converted to graphite by Fe/Zn reduction. The $\delta^{13}C$ values were measured on a dual-inlet stable-isotope mass spectrometer and are representative of $\delta^{13}C$ in the original, pre-treated sample material. The resulting conventional radiocarbon ages (CRA, years BP ± 1σ) were calibrated based on the Southern Hemisphere calibration curve SHCal13 (Hogg et al., 2013), carried out using OxCal v4.2.4 (Bronk Ramsey et al., 2013), and are presented here as a 95.4% probability range (cal. AD/BC) (Table 1).

SEDIMENTARY FACIES ASSOCIATIONS

The upper Huis River sediments were grouped into twelve sedimentary facies (Fig. 2) and five sedimentary facies associations (Table 1). The distribution of the facies associations is schematically illustrated in Figures 3 and 4A, and Figure 4B shows the stratigraphic complexities of the facies associations in the confluence region. A contrast exists in abundance and spatial distribution of FA-B, FA-C, and FA-E in bedrock-confined canyon and in the confluence region, where, except for FA-C, all other facies associations are present (Figs. 3, 4). The chief characteristics of the facies are shown in Figures 5, 6, 9, and 10; some process interpretations are illustrated in Figures 7 and 8, whereas their overall sedimentary evolution is graphically summarized in Figure 11.

Facies Association A: Massive to Graded Clast-Supported Breccias

Description.--- Facies Association A (FA-A; Table 1) is found only in the confluence area (Figs. 1, 3A). It forms discontinuous lenses that are confined to Nardouw Subgroup bedrock-protected niches and gradually becomes thinner to the west; it is invariably overlain by an erosional contact either with FA-B and FA-D (Fig. 4A). The lowermost facies in FA-A is a clast-supported, massive gravel (facies Gcm) that can be up to 1.2 m thick (Figs. 2, 4B, 5A). The medium pebble- to cobble-size clasts are mostly very angular quartzites (Fig. 5A). Tabular clasts, with long axes trending west, show imbrication in localized, vague clusters. No charcoal content was observed. The basal facies Gcm is invariably overlain by 10–20 cm thin, matrix-supported, normally graded gravels of facies Gmg, which grade into matrix-supported massive gravels (facies Gmm) with matrix content between ~ 10% and ~ 80% (Figs. 2, 5B). The matrix is composed of an organic-matter-rich, fine- to medium-grained sand.

Interpretation.--- Clast-supported, imbricated massive gravels (facies Gcm) represent the deposits of noncohesive, pseudoplastic debris flows with low matrix strength (cf. Miall, 1996; cf. Liu and Cui, 1999). Clasts imbrication suggests a paleoflow direction from east to west, and the clast orientations are typical of debris flows where clast-clast or clast-matrix collisions force elongate particles into positions of least resistance to flow, resulting in long-axis orientation parallel to the flow direction (cf. Karatson et al., 2002). The grading of facies Gcm to facies Gmm, through facies Gmg, suggests that facies Gcm of FA-A represents the bedload of a larger debris flow. The overlying matrix-supported massive gravels (facies Gmm) are indicative of high-strength debris flows (Miall, 1996), which is the natural genetic succession following a low-strength debris flow.

High-energy depositional processes are indicated by the large clast sizes in FA-A. Rare rounded clasts in otherwise immature sediments indicate the reworking of older, traction-load alluvium and more recent, less mature colluvium into the debris flow. The short travel distance indicated by the overall immaturity of FA-A as well as the westward-pointing (long axis) imbrication and thinning of facies Gcm collectively suggest that the tributary, rather than the upper Huis River, was the source of this debris flow (Figs. 1, 11.2, 11.3).

Facies Association B: Heterogeneous Matrix-Supported Breccias

Description.--- Facies Association B (FA-B; Table 1) is the thickest and most widely distributed unit of sediments in the study area (Figs. 3B, 4). A maximum thickness of eleven meters is preserved against the northeast canyon wall, although it thins out in the up-canyon direction and is not present on the southwest canyon wall (Fig. 3). Except where it overlies FA-A at the confluence, FA-B is in direct and erosional contact with the bedrock in all outcrops (Fig. 4). In the bedrock canyon, FA-B often occurs as a 0.2-0.5-m-thick, sporadic coating that plasters the canyon walls, and its horizontal, upper limit is marked by a very sharp change in the vegetation density (Fig. 10C). Two zones are clearly observable in FA-B: 1) a lower, vertically extensive unit dominated by matrix-supported breccias and 2) an upper graded unit of ~ 1 m, which is absent in the confluence area.

Lower Unit

The lower deposits of FA-B are predominantly massive matrix-supported gravels (facies Gmm) (Fig. 5C) with variable amounts of charcoal and larger (> 10 cm) clasts than facies Gmm of FA-A. In a downstream and upward directions, a poorly defined decrease in large clast size and abundance is observed. Sorting in facies Gmm of FA-B is very poor, with very angular clasts of Nardouw Subgroup quartzite and quartz veins, varying in size from very coarse-grained sand to boulders of < 64 cm (Fig. 5C). Medium to coarse pebbles are the dominant clast size throughout the lower unit of FA-B. Matrix content of facies Gmm in FA-B varies from 75% to 90% and is composed of an organic-matter-rich, fine- to medium-grained sand.

In facies Gmm of FA-B, localized clast-rich and clast-poor patches are present (Fig. 5D). These patches commonly transition laterally into beds of matrix-supported stratified gravels (facies Gms) with an internal stratification defined by vertical variation in relative abundances of graded clasts on small (Fig. 5E) and large (Fig. 5F) scales. Prominent, stratified charcoal-rich horizons are also present in facies Gms (Fig. 5E).

Associated with the largest clasts in facies Gmm of FA-B is a half spindle-shaped “linear circling” feature (*sensu* Liu and Cui, 1999) that is 2.5 m in length and 1 m in thickness (Figs. 6A, 6A’). In this feature, which is a shadow effect in the lee of the largest clasts, the concentration of pebbles, which appear to be imbricated, increases around the edges of the largest clasts on their upstream side. On the downstream side, the pebbles form two distinct bands of facies Gms that run downstream away from the large clast and merge after ~ 1.5 m, forming a single high-clast-concentration zone of Gmm. Clast content between the bands before the merger appears to be relatively high compared to the facies Gmm above and below the feature.

In the confluence area (Fig. 1), deposits of the facies Gms are not evident, but a number of matrix-supported massive sandy gravel (facies SGmm) lenses of coarse-grained sand with coarse pebbles are present (Fig. 6B). Although clast sorting is poor, it is better developed than that of facies Gmm of FA-B. These lenses of facies SGmm range in thickness from 5 to 15 cm and in length from 30 cm to 1.5 m. Due to poor conditions of exposure at the confluence, it is unclear whether or not these lenses of facies SGmm in FA-B grade into clast-rich facies Gmm as is the case with facies Gms up-canyon.

Upper Unit

The upper ~ 1-m-thick unit of the FA-B displays a distinct normal grading in the canyon (Fig. 1). Facies Gmm is overlain by normally graded, matrix-supported sandy gravels (facies SGmg), which grade into massive sands (facies Sm). Facies SGmg displays normal grading (from fine pebbles to coarse-grained sand), and vertical decrease in clast abundance, from 30% to 0% clast content. The clast composition is identical to that in the lower unit of FA-B. The overlying facies Sm is particularly rich in charcoal granules and fine pebbles (Fig. 2).

Surveying of the upper surface of FA-B revealed that its average downstream gradient is ~ 3 cm/m, ranging from ~ 7 cm/m opposite the cave and then quickly levelling to between 1.4 and 2.1 cm/m for most of the bedrock canyon. Along the same stretch of the canyon, the present-day upper Huis River bed has a gradient of ~ 6 cm/m and is thus significantly steeper than the upper surface of FA-B.

Interpretation.--- Facies Gmm of FA-B is characteristic of high-matrix-strength debris flows (cf. Miall, 1996). This is further supported by the low maturity of the sediments, the angular clasts, and the presence of large boulders throughout the deposit. The settling of large clasts, resulting in crude downstream and vertical grading in facies Gmm, is typical of cohesive debris flows (cf. Takahashi, 1991; cf. Miall, 1996; cf. Hungr, 2000).

However, the lateral and vertical facies variations (Fig. 5D) indicate a complex depositional history for the heterogeneous FA-B. The presence of facies Gms, the localized zones of inverse and normal grading in facies Gmm, as well as variation in clast content are features indicative of transitional debris flows (cf. Liu and Cui, 1999). Nonetheless, standard sedimentation models of transitional and cohesive debris flows cannot account for the complex lateral heterogeneity of the above listed features.

Hungr (2000) notes the existence of transitional fluids in some debris flows, a state that occurs when solid particles become suspended in such a manner as to behave as part of the fluid phase. The change in this relationship between solid and fluid phases can create rapid changes in viscosity of the paleoflow (Hungr, 2000). Zones of lower viscosity, and thus lower shear stress, created by the presence of transitional fluids, would facilitate the migration of large clasts from the more viscous zones, concentrating clasts in the zone of the transitional fluid. An example of this would be the concentration of clasts in the bands of facies Gms. This would create the variable features seen in FA-B that are typical of transitional debris flows. Additionally, two types of sedimentary macrostructures, identified as characteristic of transitional debris flows by Liu and Cui (1999), are also present in FA-B: (a) the “linear circling” feature (Fig. 6A) and (b) inverse-to-normal grading (in facies Gms; Fig. 5E). The low gradient of the upper surface of FA-B further supports the transitional properties of this debris flow, as transitional flows have been noted to form flat-topped deposits (Liu and Cui, 1999). Moreover, the clast-rich zones of facies Gmm and Gms, the charcoal-rich strata in facies Gms and the zones of consistent clast size in facies Gmm and Gms possibly also resulted from a transitional phase in an otherwise cohesive part of the debris flow, rather than separate paleoflows.

It is thus possible that FA-B is the deposit of a relatively dry debris flow, with fluid content sufficient to place it in the transitional-debris-flow category. Zones of anomalous internal pressure created the localized transitional fluid concentration, which in turn resulted in the bimodality of the drier cohesive zones and less viscous transitional zones. All of these features indicate that FA-B represents the deposits of a transitional debris flow, closer to the cohesive part of the spectrum.

At the confluence (Fig. 1), the FA-B differs from that in the canyon, in that facies Gmm does not display the variation in clast abundance or transitions to facies Gms. Here: 1) the presence of laterally extensive facies SGmm lenses in facies Gmm (Fig. 6B); and 2) the relatively sharp contact between facies Gmm and SGmm, in contrast to the gradational transition from facies Gmm to Gms in the canyon, indicates that these lenses resulted from the overlap of successive cohesive debris flows. For example, the lenses of facies SGmm could overlie facies Gmm of the precursory surge (Figs. 7, 11.4, 11.5), and in turn be overlain by deposits of the debris flow that overshot the debris-flow front (Figs. 7C, 11.7). Such surges or pulses are reported from several case studies on debris flows (Costa and Williams, 1984; Cannon et al., 1998).

The upper unit of FA-B demonstrates distinct normal grading in the matrix-supported sandy gravels (facies SGmg) to massive sands (facies Sm), which stands in contrast to the transitional debris-flow sediments of the lower unit of FA-B. When the debris flows rapidly decelerated and stopped in the bedrock canyon (Fig. 11.5), the relatively flat upper surface of the transitional debris flow was probably overridden by less cohesive flows (Fig. 11.6, 11.7, 11.8) as sediment concentration in the tail floodwaters decreased (Fig. 7D). Deposition may have continued to take place on top of debris flow sediments (cf. Takahashi, 1991), and this is likely represented by the transition zone where the pure debris flow deposits (facies Gmm) grade into an inertial and traction carpet layer beneath the overlying (and in this case unpreserved) hyperconcentrated flow (cf. Costa and Williams, 1984; cf. Sohn et al., 1999; 2002). The normal grading also indicates a transition from a cohesive mature debris flow, represented by facies Gmm in FA-B, to an immature debris flow (cf. Takahashi, 1991). The reason for this could be that the flow bed surface of the overriding surge (the facies Gmm sediments of the earlier surges) had a shallower gradient than the main debris flow (cf. Takahashi, 1991). This inference is supported by our land survey results presented below.

Numerous lines of evidence indicate that the main front of the FA-B debris flow was stopped at the first major bend of the bedrock canyon (Fig. 11.4, 11.5), at the transition from canyon into the confluence zone (Fig. 1). First, in the canyon, FA-B is up to ~ 12 m thick, with a nearly level upper surface (Fig. 10C), but this sediment package rapidly declines to a thickness of ~ 1 m in the confluence zone. The transition area, which is an extremely narrow constriction of the canyon, has no *in situ* sediment (see gap in Fig. 4A) and exposes an eroded bedrock spur, provides an ideal setting for the process of debris-flow-front stopping (Fig. 7). This is because here a major reduction in channel-floor gradient occurs as the narrow constriction (i.e., bottleneck) widens into the confluence. Takahashi (1991) also noted that channel-confined debris flows rapidly decelerate and stop (i.e., freezes) when the channel levels out. Furthermore, as fluids are lost during downstream flow, debris flows cohesively freeze as a result of increased internal friction (cf. Costa, 1984; cf. Shultz, 1984; cf. Miall, 1996), and the presence of structures interpreted to be a zone of colloidal transitional fluid flow could indicate that constant fluid removal was taking place.

Facies Association C: Coarse-Grained Sands

Description.--- Facies Association C (FA-C; Table 1) is limited to a small outcrop ~ 11 m above the present river channel in a canyon-wall cave, which has formed by the collapsing of the core of an antiformal fold closure in the host quartzites (Figs. 1, 3C, 4A). The cave sediment, found only on the floor of the cave, is less than 10 m in length and reaches a maximum thickness of 1.2 m. It comprises massive, organic matter-rich (> 10%), sandy detritus (facies Om), with a < 10% matrix of very fine-grained quartz sand and silt (Fig. 2). Two ~ 50-cm-wide and 5 – 20-cm-thick lenses of open-framework, clean, massive coarse-grained sands (facies Smo) are also contained in facies Om (Fig. 2). Grains in these lenses are mostly angular to subrounded quartz and < 5% charcoal content. The lower lens comprises well sorted, coarse-sand-size quartz grains, whereas the upper lens is moderately sorted with quartz grains ranging in size from fine- to coarse-grained sand. A further 60-cm-thick package of planar laminated organic detritus (facies Ol) overlies facies Om (Figs. 2, 6C). This consists of 0.5–20-mm-thick, planar laminated, blade- and needle-shaped, granule-size charcoal grains, commonly preserving plant fragments (e.g., twigs) and rare rounded charcoal clasts. Very fine-grained, subangular quartz sand comprises the matrix, which is ~ 5% of the deposit. Several very angular cobbles and boulders of Nardouw Group quartzite (Fig. 6C) are embedded into facies Ol with lithology identical to the quartzites in the cave wall.

Interpretation.--- The fine-grained sediments in the cave are interpreted here as mainly slackwater deposits (cf. Baker, 1987) that partially formed from traction currents (facies Smo) and settled out in a small, cave-confined water body (facies Om and Ol), whereas the very rare, very angular, large quartzite clasts (Fig. 6C) are considered *in situ* fragments that had fallen from the ceiling of the cave into the slackwater deposits.

It is likely that the slackwater sediments in the cave did not form during the same flood that generated FA-B because: (a) the base of FA-C sediments is below the level of the top of the FA-B (Fig. 4A) and (b) FA-B predates FA-C by about ~ 500 years (see Radiocarbon ages section). Possibly some sediments were deposited in the cave at the time when FA-B was formed, but most likely subsequent erosional process removed sediments of FA-B age from the cave (Fig. 8A). Consequently, the deposition of FA-C in the protected hollow of the cave had to be predated by a major scouring event (Fig. 11.8) that would have: (a) lowered the overall surface of the debris-flow sediments filling the bedrock canyon by incising into FA-B; and (b) flushed out sediments of FA-B from inside the cave (Fig. 8A).

Arguably, the protected nature of the cave setting does not provide an ideal environment for sustained water flow, making not only the erosion of FA-B sediments but also the presence of traction current deposits (facies Smo) highly anomalous. Smith et al. (2011) noted that the impact of a water current against a resilient surface can divert as much as a third of the current back upstream, creating an anticlockwise eddy with a maximum erosional ability during peak paleoflow. In our case, the downstream cave wall may have acted as the resilient surface, and the erosional ability of the resultant anticlockwise eddy could have allowed: (a) the scouring of the FA-B sediments from the cave; (b) keeping in suspension even the coarser-grained sandy sediments; and (c) trapping the charcoal as a floating surficial mat on the top of the eddy current in the cave. It is noteworthy that although this flow-separation model was presented for downstream-migrating point bars, its application to caves has not been tested in sedimentological studies on internal circulation of sediment-laden waters in caves.

Although the possibility that at least some of the charcoal in the cave sediments was generated by human fire activity in the cave exists, sedimentological evidence for this is lacking. However, irrespective of the source of the charcoal in the cave sediments, experiments on waterlogging of charcoal are important to be considered for their depositional dynamics in the slackwater sediments. Nichols et al. (2000) demonstrated that the unique transport and depositional dynamics of charcoal is a function, among other factors, of the (a) variable charring properties of different plants and plant parts, and (b) the variable waterlogging rates of different-sized charcoal fragments. It is therefore reasonable to assume that the buoyant, sand-size charcoal fragments took time to became waterlogged and only settled out with their hydraulically equivalent, higher-density, silt-size lithic or mineral fragments. Thus as Figure 8 depicts, deposition in the cave commenced as the sediment-loaded eddy current would decrease in energy, causing the rapid deposition of the coarser-grained, charcoal-free sand first (facies Smo), followed by the mixture of finer-grained sand and, by then waterlogged charcoal fragments to settle rapidly as a massive organic-matter-rich detritus (facies Om) (Figs. 8C, 8D). Facies Ol represents a final phase of low-energy, suspension settling in pools of standing water in the cave (Figs. 8E, 8F). In this interpretation, FA-C represents a sequence of depositional processes, characteristic of bedrock-confined settings subject to multi-peak paleofloods or recurrent paleoflooding events.

Facies Association D: Bipartite Grit and Sand with Subordinate Clast-Supported Breccia

Description.--- Facies Association D (FA-D; Table 1) is extensive throughout the distal part of the study area (Figs. 3D, 4, 6) and comprises discrete depositional packages, consisting of clast-supported massive gravel (facies Gcm), overlain by a layer of matrix-supported, inversely graded sandy gravel (facies SGmi), succeeded by massive sand (facies

Sm) and finally covered by a unit of laminated organic-matter-rich detritus (facies Ol) (Fig. 6D).

Facies Gcm forms channel-shaped lenses that are overlain by laterally continuous layers of facies SGmi and Sm (Fig. 9A). Facies Gcm comprises angular fine pebble- to cobble-size clasts of Nardouw Group quartzite and vein quartz, with small amounts of rip-up clasts, and ~ 10% of sandy matrix. Medium- to coarse-pebble-size clasts are common, and the maximum clast size in these lenses is 18.4 cm. Subrounded rip-up clasts (Fig. 9B) also appear in facies Gcm, and are possibly sourced from the sediments of the underlying FA-B. Imbrication suggests variable westward- and eastward-directed paleoflow directions. No charcoal was observed in the matrix of facies Gcm.

The overlying facies SGmi (Fig. 9C) is poorly sorted, with clasts typically ranging from medium-grained sand to granule size, although occasional isolated clasts of up to cobble size are also present (Fig. 9D). Vertically, there is a decrease in matrix content from 70% to 40%. Randomly oriented charcoal clasts are common. Rare, up to 10-cm-thick lenses of clast-supported, angular quartzite pebbles (Fig. 9E) are preserved at the contact between facies SGmi and overlying facies Sm. The clast imbrication in these lenses indicates a paleoflow direction to the north, parallel to the flow direction of the present-day upper Huis River. These lenses appear to increase in size and abundance towards the southern part of the confluence area (Fig. 3). Both facies Gcm and SGmi have erosional bases and are incised into the underlying sediments (Figs. 4B, 9F).

Closely associated with and invariably overlying facies SGmi, the beds of facies Sm (Fig. 2, 4B) are richer in charcoal clasts and consist of a typically organic-matter-rich, dark gray sediment with < 10% medium- and coarse-grained sand in a matrix of very fine-grained quartz sand and silt-size organic debris. A total of seven SGmi-Sm facies couplets have been identified in the best exposure of FA-D. The finest facies of FA-D (facies Ol) forms discontinuous lenses along the upper surface of facies Sm. Facies Gcm and Ol are not preserved in association with every SGmi-Sm facies couplet.

Interpretation.--- Similar to FA-A, the basal units of some of the FA-D packages (facies Gcm) are interpreted as products of pseudoplastic debris flows with low matrix strength (cf. Miall, 1996). Facies Gcm may have been the bedload of the small sediment gravity flows that produced the overlying matrix-supported inversely graded sandy gravel (facies SGmi) layers. This would explain why large clasts in the rest of FA-D and charcoal fragments in facies Gcm are very rare. This interpretation is consistent with immature debris flows, as described by Takahashi (1991).

The scoured lower surfaces of the facies Gcm deposits likely represent pre-existing erosion surfaces of the river, and were not produced by the events that formed facies Gcm. This is supported by: (a) the paleoflow directions of facies Gcm being at a sharp angle to the canyon walls – a situation that would likely occur if the sediment flow that produced facies Gcm was forced into pre-existing channels (i.e., scoured river bed); and (b) the presence of subrounded rip-up clasts of FA-B in the otherwise angular clasts of facies Gcm, which suggests that fragments ripped-up from FA-B endured attrition, a process incompatible with sediment gravity flows. These features imply periods of sustained paleochannel flow and associated processes (scouring, clast attrition) between sediment-gravity-flow events, which then recurrently exploited these streamflow-carved paleochannels (Fig. 11.10, 11.13).

Bipartite layers, similar to SGmi-Sm facies couplets, have been noted in other examples as the potential hallmark features of hyperconcentrated flows (cf. Miall, 1996; cf. Sohn et al., 1999; cf. Benvenuti, 2003), which also have a tendency to move larger clasts to edges of the paleoflow where the shear stress is lower, resulting in inverse grading such as that observed in facies SGmi. The facies characteristics (e.g., paleoflow direction, spatial distribution) of the imbricated pebble lenses found at the contact between facies SGmi and Sm (see Fig. 9E) can suggest that these lenses originated from the gravity winnowing (cf. Postma, 1984) of the older FA-B debris-flow sediments situated farther to the south.

Massive sands (facies Sm) are interpreted as sediment gravity flows (cf. Miall, 1996). These deposits contained randomly oriented large charcoal fragments (Fig. 2) and other larger clasts, which also imply that these are not secondary massive fabrics due to postdepositional modification (e.g., bioturbation, pedoturbation).

The rare large clasts, up to 20 cm, in facies SGmi and Sm (Fig. 7D) indicate high peak energy levels associated with the deposition of these facies, which is further supported by the presence of the erosional contact at the base of each SGmi-Sm facies couplet (Fig. 7A, D, F). This erosional nature could also explain the spatial distribution of the SGmi-Sm facies couplets, which are laterally more continuous in the eastern parts of the confluence area (Figs. 1, 6D), but tend to form lenses to the west (Fig. 7D). To the west, where younger FA-D depositional events eroded older facies, paleoflow from both the upper Huis River and its tributary would have exited to the confluence. However, to the east, as these currents merged, there may have been some backwashing and lowering in the energy of the paleoflow, leading to the deposition of SGmi-Sm facies couplets.

The planar lamination of charcoal in facies Ol lenses suggests deposition from suspension under low-energy conditions in a final depositional pulse (Fig. 11.13) of the events that generated the SGmi-Sm facies couplets. Furthermore, these lenses, found at the sharp contact between facies Sm and succeeding facies SGmi, are interpreted here as the eroded remnants of more laterally extensive layers of facies Ol. To summarize, facies Ol are a series of slackwater deposits (cf. Baker, 1987) that covered a larger area at the confluence, which would have been an ideal setting for a sudden reduction in paleoflow velocity of currents from all directions due to the abrupt widening of the river channel in this area. The preservation of facies Ol in lenses, rather than in laterally continuous layers, may be linked to the high likelihood of slackwater deposits being eroded once the system returns to normal paleoflow conditions (cf. Baker, 1987). The multiple SGmi-Sm facies couplets and associated lenses of facies Ol containing buoyant charcoal (e.g., Fig. 6D) may be indicative of recurrent paleoflooding events or multi-peak large paleofloods. Constraining the number of lower-frequency, major depositional events might be possible with a systematic radiocarbon dating of charcoal in FA-D.

In summary, FA-D represents the deposits of sediment gravity flows with: (a) the basal facies Gcm being the bedload of low-matrix-strength debris flows that occupied pre-existing channels (Fig. 11.12); (b) the couplets of facies SGmi-Sm being the deposits of hyperconcentrated flows, unconfined by the channels and spreading laterally across the confluence (Fig. 11.12); (c) the imbricated pebble lenses being the gravity winnowing of the FA-B debris-flow front (Fig. 11.11); and (d) facies Ol being the slackwater deposits, produced when the paleo-floodwaters receded (Fig. 11.13).

Facies Association E: Massive Sands and Imbricated Clast-Supported Conglomerate/Gravel

Description.--- Facies Association E (FA-E; Table 1; Figs. 3D, 4A, 10) forms a series of clast-supported, subangular to rounded, imbricated gravels (facies Gcb); massive organic-matter-rich sands (facies Sm) and subordinate facies Gmm (Fig. 10). The eroded remains of facies Gcb form a semiconsolidated gravel mantle that armors the upper eroded surfaces of

FA-B and FA-D (Figs. 4A, 10A). Additionally, in two instances, imbricated boulder bars (facies Gcb) comprising poorly sorted, subrounded to subangular clasts up to ~ 1 m in diameter and separated by patches of massive sand (facies Sm) are considered here as part of FA-E (Figs. 3D, 10C, 10D, 10E, 10F). Boulder size generally decreases down the bar but remains very large (0.3–0.4 m intermediate diameter) in Boulder Bar 2 in the bedrock canyon, and decreases markedly towards the downstream end and margins (down to 0.05 m intermediate diameter) in Boulder Bar 1 at the confluence (Fig. 3D). Boulders often show crescentic attrition (“chatter”) marks on their surfaces (Fig. 10F). Most boulders are subangular to subrounded quartzites from the Nardouw Subgroup (Table Mountain Group), and only a few boulders are rounded clasts of conglomerates, diamictites, and dark pyritic siltstones and shales (probably from the nearest outcrops that are ~ 5-6 km upstream; Fig. 1).

The FA-E packages that rest on the FA-B deposits in the bedrock canyon range in thickness from ~ 30 cm to ~ 1 m and are dominated by facies Sm with abundant lenses of facies Gcb (Fig. 10B). The facies Sm is composed of well sorted, fine- to medium-grained sand, with charcoal clasts occasionally reaching granule size. The ~ 10-cm-thick and ~ 1-m-long lenses of facies Gcb are typically composed of subangular to subrounded clasts with sizes ranging from 2 mm to 15 cm. Some of the lower Gcb lenses in FA-E consist of angular clasts. Most of these gravel lenses display imbrication (Fig. 10B) and indicate a paleoflow direction identical to that of the modern upper Huis River.

In addition, FA-E also overlies FA-D at the confluence and at lower elevations of the canyon walls (see the northern and central parts of Fig. 4A). In these outcrops, which are typically small and thin and contain only a single lens of facies Gcb, the clasts are slightly more rounded and marginally better sorted that those in the upper part of the bedrock canyon.

Interpretation.--- The sediments of FA-E are traction-load products in variable-energy streamflows that were confined to the upper Huis River channel. The subrounded and imbricated gravels (facies Gcb; Fig. 10A) are formed in channel gravel bars that resulted from attrition in sustained paleo-streamflow processes during ordinary paleofloods. Facies Sm represents the rapid deposition of sand probably sourced from farther up the catchment or via reworking of the matrix of exposed FA-B. The vertically stacked lenses of facies Gcb in facies Sm suggest that the fluvial system that deposited FA-E in the bedrock canyon was episodically aggradational (Figs. 4A, 11.10, 11.11) (cf. Nanson, 1986). The protective effect of the semiconsolidated gravel mantle of FA-E that armors FA-B and FA-D has been shown to limit erosion in bedrock-confined rivers (cf. Finnegan et al., 2014).

The large clast size of the subrounded to subangular and imbricated boulders in the two upper Huis River bars testify to attrition in currents with extraordinary erosive powers (Figs. 11.14, 11.15) during the two extreme paleofloods, some ~ 900 and ~ 650 years ago (see Table 1 and next section). These catastrophic paleoflood events stripped clean (i.e., flushed out) most of the bedrock canyon (cf. Nanson, 1986), abraded and plucked the exposed bedrock, churned the large clasts in bedload, and then finally deposited them as boulder bars. The aftermath of these powerful scouring events are the erosional remnants of the older facies that only remained intact, often just as a patchy plaster against the canyon walls (Fig. 10C).

RADIOCARBON AGES OF THE FACIES ASSOCIATIONS

Radiocarbon analyses of charcoal fragments from FA-B (Table 1) in the bedrock canyon indicate that the age of this facies association is 363–108 cal BC (2165 ± 35 BP, SUERC-35169 BAR-D). The sample from the upper part of FA-C (Table 1) in the cave yields an age range of 341–539 cal AD (1628 ± 37 BP, SUERC-36432 BAR-C), and thus facies Ol of FA-C in the cave is ~ 500 years younger than the canyon-filling FA-B sediments. This is noteworthy because: 1) the relative dating of FA-C is not possible as it is confined to the cave that is ~ 11 m above the present river channel and isolated from the outcrops of other facies associations; and 2) our high-precision land-survey results show that the base of FA-C is 1.06 m below the upper surface of FA-B that is preserved in outcrops along the opposite canyon wall (Figs. 1, 3, 4A). Radiocarbon analyses of samples from facies Sm in FA-E (Table 1) preserved in the large boulder bars suggest that Boulder Bar 1 at the confluence area (Figs. 1, 3D) date to 1039–1216 cal AD (894 ± 37 BP, SUERC-36431 BAR-B), whereas Boulder Bar 2 in the bedrock canyon (Figs. 1, 3D, 10) is younger, yielding an absolute age of ~ 1300 AD (653 ± 35 BP, SUERC-35166 BAR-A), with calibrated ages ranging between 1277–1329 cal AD (45.1% probability) and 1341–1396 cal AD (50.3% probability).

The volumetric abundance of the charcoal in the five facies associations is variable (with FA-B having the highest charcoal content and FA-A containing no charcoal). The charcoal is usually randomly distributed; however, it forms discrete or crude layers in FA-B and FA-C, and clusters in FA-D. Each radiocarbon-dated charcoal sample (Table 1) is composed of many individual charcoal fragments, and therefore it is possible that each sample age represents an average of several different ages (i.e., different fires), because charcoal can be reworked. However, the sampled charcoal fragments were not only angular to very angular and elongated, but also fragile and presumably less likely to have been reworked in traction processes (cf. Nichols et al., 2000). In response to in mass-movement processes, charcoal is typically moved *en masse* without being abraded or attired (cf. Muir et al., 2015), and the shape of the fragments in debris-flow deposits (e.g., FA-B or facies Sm in FA-E) remains unchanged even after multiple mass-movement events (i.e., reworking from the burned catchment). For these reasons, the radiocarbon-dated charcoal samples are considered to provide a reliable discrete, nonetheless average, age for the facies associations. The consistency of the absolute ages is confirmed by the relative ages of the various facies associations that were determined from their stratigraphic relationships (Fig. 4).

PALEOFLOOD HYDROLOGY

The paleoflood sediments are found up to ~ 12 m above the floor of the present river channel along the canyon walls and in the cave. Together with the large-boulder bars in the main channel of the upper Huis River, the relative positions of these deposits, established in our land surveying, were applied in some semiquantitative hydraulic estimates of the peak flow during the paleofloods (Table 2). The formulae of Riggs (1976) and Williams (1978) for within-bank or bankfull discharge were used as they are most applicable to bedrock canyons. Both equations require knowledge of the geometric parameters of the bedrock canyon for cross-sectional flow area and longitudinal channel slope (gradient), which were obtained with in the field via surveying and confirmed using Google Earth. For the measurement of the three cross sections in the bedrock canyon (Table 2), the estimation of the maximum depth value was guided by the height of the slackwater deposits (FA-C) from the channel floor as well as the maximum thicknesses of FA-B, which invariably coincides with the abrasion mark or scour line on the canyon wall (Fig. 10C).

The results of the paleo-discharge calculations are presented in Table 2, but it should be noted that these hydraulic paleoflow calculations in the bedrock canyon of upper Huis River are of limited precision for several reasons (Williams and Costa, 1988). These include the meandering nature of the channel, the non-uniform shape of the cross sections, and the irregularities in the channel floor. The latter include prominent potholes and a waterfall and plunge pool with a combined throw of at least 5 m is present near the upstream end of the canyon. Most channel floor irregularities are due to the thick-bedded (± 1 m) nature of the bedrock quartzites, which tend to part along bedding planes and orthogonal joints.

The equations of Riggs (1976) and of Williams (1978) gave paleoflood discharge estimates of 4014 m^3/s and 3048 m^3/s, respectively. These discharge values are particularly applicable to the paleofloods that generated and removed most of FA-B from the bedrock canyon. They are comparable to the paleo-discharge estimation based on Costa's (1983) approach, where the mean flow velocity (*V*) and the average length of the intermediate axis of the five largest boulders (*d*) are considered (Table 2). The latter value (*d*) is ~ 1 m in boulder bar (FA-E) close to the cross sections. However, it should be noted that the error in applying this formula is estimated at between 25 and 100% (Williams and Costa, 1988).

The lower discharge value of 2326 m^3/s obtained with Costa's (1983) approach is expected, because the boulder bars form when the flood velocity decreases (and not at peak discharges). The wide range in paleo-discharge values is testimony to the crudeness of the calculation processes, and they must therefore be regarded as raw estimates. Nevertheless, the values obtained suggest extreme paleo-discharges for multiple paleoflood events in the upper Huis River, which has a catchment of approximately 25 km^2 in size. As a comparison, the magnitude of the January 1981 flood at Laingsburg, the largest modern flood in the region's flood record in the past 100 years, was associated with a discharge of 5700 m^3/s for the Buffels River and 11000 m^3/s for the Groot River, which have a total catchment area of 4000 km^2 and 12500 km^2, respectively (Zawada, 1994).

DISCUSSION

The link between recurring wildfires and massive sedimentation events have considerable importance for the evolution of the landscape and biota (e.g., Belcher et al., 2013; Muir et al, 2015). Although regular wildfires in the fire-prone and fire-dependent Fynbos Biome are key ecological elements in revitalizing and sustaining one of the highest plant biodiversities in the world (Allsopp et al., 2014), catastrophic mass-wasting events are rare in the region. These mass-wasting events occur mainly after those large wildfires that are followed by rare, extreme rainfall events, and which occur before the revegetation of the steep catchment slopes (Scott, 1993; Moody et al., 2013). It is possible that a similar chain of events induced the development of the sedimentary facies of the upper Huis River (Fig. 11), in particular in the case of the up to 12-m-thick pile of FA-B sediments, which were generated in a single, large-magnitude debris flow some ~ 2000 years ago (Figs. 11.2, 11.3, 11.4), and which were likely triggered by a low-frequency, but high-magnitude paleoflood. However, firmly linking even this large paleoflood to an immediately preceding, single, discrete major fire is hazardous. This is because the bulk dated charcoal samples provide only average ages (see section on "Radiocarbon ages") that are unsuitable proxies for the frequencies of past fires or the actual age of the sedimentation event that finally entombed the charcoal in FA-B. In other words, the dated charcoals in FA-B might not be primary, and could have been: 1) generated in several moderate fires; 2) stored in the burned catchment; 3) locally mobilized via post-fire colluvial (e.g., surface runoff, soil creep) processes; and 4) brought, mainly *en masse*, into the canyon later by a major devastating paleoflood. Therefore it is possible that FA-B sediments formed in a paleoflood that occurred after a particularly long fire-free period combined with a severe drought, which would have promoted: 1) the thickening of the unconsolidated weathering blanket over the catchment (e.g., no surface runoff); and 2) the accumulation of dry, flammable plant biomass. Accumulations of plant biomass can be an important fuel for deeply penetrating, severe and intense surface fire, which among others, destroys ground covering (soil binding) vegetation, reduces infiltration, and promotes hydrophobic soils (cf. Meyer et al. 1995; Whitlock and Larsen, 2002).

Consequently, estimating the number or periodicity of paleofloods and fires in the upper Huis River catchment is possible only in the most general terms based on the obtained charcoal ages (i.e., ~ 2165, 1628, 894, 653 BP). Because the charcoals postdate the arrival of pastoralists in southern Africa some 2000 years ago (Schapera, 1930; Hall, 1984; Sealy and Yates, 1994; Henshilwood, 1996; Seydack et al., 2007; Kraaij and van Wilgen, 2014; Sadr, 2015), the possibility of anthropogenic ignition (or even wildfire suppression) cannot be excluded. Firmly establishing the recurrence interval of these events over the ~ 1500 years is also complicated by the possibly that an indefinite number of floods and fires may have been unrecorded in the natural archives of the sediments due to their low preservation potential in bedrock canyons like the upper Huis River.

Furthermore, the charcoal-free FA-A indicate that fires were not always essential for debris-flow generation in the study area. On the other hand, the debris-flow deposits of FA-A (Fig. 11.3) also confirm a large discharge event considering the relatively small size of the tributary catchment, in relation to the 25 km^2 catchment of upper Huis River upstream from the confluence. Although the deposits of FA-A are overlain by those of FA-B with a sharp contact (Fig. 4B), the possibility exists that both of these debris flows resulted from the same extreme discharge event, but the debris flow responsible for FA-A reached the confluence first, having a closer source as well as being wetter and thus faster due to lower viscosity (Fig. 11.4). If FA-A and FA-B are coeval, the absence of charcoal in FA-A might also be due to the lack of fire in the tributary catchment before the extreme paleoflood.

Unquestionably, in the study area the most powerful and erosive events were the cataclysmic paleofloods that generated the two boulder bars of FA-E (Fig. 11.15). Textural characteristics and composition of the boulder bars (Fig. 10C-F) indicate that: a) charcoal is most likely primary; and b) the paleoflood water could incise through the older facies associations and into the bedrock, and was able to flush the valley nearly clean. The clasts from the scoured bedrock were deposited as boulder bars in the confluence area earlier than in the bedrock canyon (Figs. 3D), and this age discrepancy of well over 150 years (and up to 300 years; see Table 1) can suggest that fluvial back-cutting and/or down-cutting took place from northwest to southeast in at least two discrete high-magnitude, low-frequency paleofloods.

Quantifying the parameters of these repeated paleoflood events (i.e., actual magnitude, intensity, duration, frequency, sediment transport capacity) from the preserved sedimentary architecture alone is rather difficult. This is not only because the site most probably preserves an incomplete alluvial record of past sedimentary events with unsteady sedimentation rates (cf. Kemp and Sexton, 2014; cf. Miall, 2014a, b), but also due to the poorly known sedimentary dynamics in bedrock-confined rivers (Jansen and Brierley, 2004). This is particularly valid for those rivers that are set in the fire-prone and fire-driven ecosystem of the Fynbos Biome, where to our knowledge only rare, preliminary reports exist on their paleoflood record (e.g., ~ 90 km east from the upper Huis River in the Gourits or Gouritz River; Van Bladeren et al., 2007). Future directions of research might provide further insight on the above listed, but lacking paleoflood parameters by improving the quality and quantity of the data on the alluvial architecture of deposits that resulted from modern, historic and prehistoric floods.

Correlation of these radiocarbon-dated, charcoal-bearing paleoflood and extreme paleoflood sediments of the upper Huis River (Table 1) to regional proxies of climate variability from the past 2000 years has been ineffective, partly due to the poorly constrained African temperature variability data (cf. Nicholson et al., 2013; PAGES 2k Consortium, 2013). The main reason why correlating the extreme paleoflood record in upper Huis River with recent climatic changes is fruitless is that these rare and unusual sediments were likely generated by high-magnitude and low-frequency weather events (e.g., summer storms) rather than long-term climatic events (cf. Baker, 2000). To date, evidence for similar debris-flow-dominated massive sedimentation events in the deeply incised valleys of the SW Cape Fold Belt remains to be discovered. However, ignoring this naturally achieved, rare, but very real paleoflood record would limit not only the constraining of the extremes in the Holocene weather in SW South Africa, but also the regional flood probability estimations, hazard predictions and mitigations in flood-prone southern Africa.

CONCLUSION

The upper Huis River sediments provide a rare window into the recent geological past by recording the response of an alluvial system to Holocene paleofloods and fires over ~ 1500 years in an area characterized by deeply incised river valleys set in a tectonically remarkably stable region (cf. Scharf et al., 2013). Detailed facies analysis of these Holocene ”accidents of preservation” (*sensu* Smith et al., 2015) has enabled the reconstruction of the depositional history of the upper Huis River since 363–108 cal BC (2165 ± 35 BP). In addition to radiocarbon dating of charcoal, sedimentological facies analysis in this study assisted in separating the Holocene stratigraphic record of the upper Huis River into several individual and different sediment transport events that represent multiple cataclysmic paleofloods (Table

1). The results also show that the normal stream paleoflow, paleoflood, and extreme paleoflood deposits in the upper Huis River valley are products of both high-frequency and low-frequency peak discharge events and associated phenomena. Radiocarbon dates indicate that major paleofire events occurred at ~ 363–108 cal BC as well as around ~ 1100 cal AD, and finally some ~ 200 years later, around ~ 1300 cal AD; however, the actual magnitude, intensity, duration, source, and frequency of these repeated paleofire events and their linkage to paleoflood events remain unconstrained. The Holocene sediments in the upper Huis River present specific insights into sedimentological and gemmological evolution of bedrock-confined rivers, where repeated events of deposition (resulting in heterogenous debris-flow deposits, boulder bars), valley scouring, and alluvium flushing occur during extreme paleofloods.

ACKNOWLEDGMENTS

The authors are grateful for the assistance provided by Laurence Matthews, Wesley Dawson, and Damon Hope in the field, Tasha Phillips on the reporting of radiocarbon dates and to Russell Hope for providing advice on high-precision surveying techniques. Research funds received by EMB from the National Research Foundation of South Africa (incentive funding) and the University of Cape Town (URC grant) are gratefully acknowledged. The funders had no other involvement in this research and therefore do not accept any liability in regard thereto. We are also grateful for the expert reviews, comments, and suggestions by one anonymous reviewer, Martin Gibling, Alessandro Ielpi, Frank Neumann, John B Southard, and associate editor Jennifer J Scott, which improved the content and presentation of the manuscript.

REFERENCES

AGER, D.V., 1973, The nature of the Stratigraphic Record: New York, John Wiley, 114 p.

ALLSOPP, N., COLVILLE, J.F., AND VERBOOM, G.A., 2014, Fynbos: Ecology Evolution and Conservation of a Megadiverse Region: Oxford, UK, Oxford University Press, 416 p.

BAKER, V.R., 1984, Flood sedimentation in bedrock fluvial systems, *in* Koster, E.H., and Steel, R.J., eds., Sedimentology of Gravels and Conglomerates: Canadian Society of Petroleum Geologists, Memoir 10, p. 87–98.

BAKER, V.R., 1987, Paleoflood hydrology and extraordinary flood events: Journal of Hydrology, v. 96, p. 79–99.

BAKER, V.R., 2000, Paleoflood hydrology and the estimation of extreme floods, *in* Wohl, E.E., ed., Inland Flood Hazards: Human, Riparian, and Aquatic Communities: Cambridge, UK, Cambridge University Press, p. 359–377.

BAKER, V.R., AND KOCHEL, R.C., 1988, Flood sedimentation in bedrock fluvial systems, *in* Baker, V.R., Kochel, R.C., and Patton, P.C. eds., Flood Geomorphology: New York, John Wiley & Sons, p. 123–137.

BELCHER, C.M., COLLINSON, M.E., AND SCOTT, A.C., 2013, A 450-million-year history of fire: *in* Belcher, C.M., ed., Fire Phenomena and the Earth System: An Interdisciplinary Guide to Fire Science, Oxford, UK, John Wiley & Sons, p. 229–249.

BENITO, G., THORNDYCRAFT, V.R., RICO, M.T., SÁNCHEZ-MOYA, Y., SOPEÑA, A., BOTERO, B.A., MACHADO, M.J., DAVIS, M., AND PEREZ-GONZALEZ, A., 2011, Hydrological response of a dryland ephemeral river to southern African climatic variability during the last millennium: Quaternary Research, v. 75, p. 471–482.

Benvenuti, M., 2003, Facies analysis and tectonic significance of lacustrine fan-deltaic successions in the Pliocene–Pleistocene Mugello Basin, Central Italy: Sedimentary Geology, v. 157, p. 197–234.

Bond, W.J., and Scott, A.C., 2010, Fire and the spread of flowering plants in the Cretaceous: New Phytologist, v. 188, p. 1137–1150.

Bond, W.J., and Van Wilgen B., 1996, Fire and Plants: London, UK, Chapman and Hall Press, 263 p.

Bradshaw, P.L., and Cowling, R.M., 2014, Landscapes, rock types, and climate of the Greater Cape Floristic Region, *in* Allsopp, N., Colville, J.F., and Verboom, G.A., eds., Fynbos: Ecology, Evolution, and Conservation of a Megadiverse Region: Oxford, UK, Oxford University Press, p. 26–46.

Bronk Ramsey, C., Scott, M., and van der Plicht, H., 2013, Calibration for archaeological and environmental terrestrial samples in the time range 26–50 ka cal BP: Radiocarbon, v. 55, p. 2021–2027.

Burke, K., and Gunnell, Y., 2008, The African erosion surface: a continental-scale synthesis of geomorphology, tectonics, and environmental change over the past 180 million years: Geological Society of America, Memoir 201, p.1–66.

Cannon, S.H., Powers, P.S., and Savage, W.Z., 1998, Fire-related hyperconcentrated and debris flows on Storm King Mountain, Glenwood Springs, Colorado, USA: Environmental Geology, v. 35, p. 210–218.

CGS (Council for Geoscience), 1997, 1:1 000 000-scale geological map of the Republic of South Africa and the Kingdoms of Lesotho and Swaziland. https://www.geoscience.org.za/images/DownloadableMaterial/RSA_Geology.pdf

Costa, J.E., 1983, Palaeohydraulic reconstruction of flash-flood peaks from boulder deposits in the Colorado front range: Geological Society of America, Bulletin, v. 94, p. 986–1004.

Costa, J.E., 1984, Physical geomorphology of debris flows, *in* Costa, J.E., amd Fleisher, P.J., eds., Developments and Applications of Geomorphology: Heidelberg, Springer-Verlag, p. 268–317.

Costa, J.E., and Williams, G.P., 1984, Debris-flow dynamics: U.S. Geological Survey, Open File Report 84–606.

Cowling, R., 1992, The Ecology of Fynbos: Nutrients, Fire and Diversity: Oxford, UK, Oxford University Press, 411 p.

Damm, B., and Hagedorn, J., 2010, Holocene floodplain formation in the southern Cape region, South Africa: Geomorphology, v. 122, p. 213–222.

Finnegan, N.J., Schumer, R., and Finnegan, S., 2014, A signature of transience in bedrock river incision rates over timescales of 10^4–10^7 years: Nature, v. 505, p. 391–394.

Florsheim, J.L., Keller, E.A., and Best, D.W., 1991, Fluvial sediment transport in response to moderate storm flows following chaparral wildfire, Ventura County, southern California: Geological Society of America, Bulletin, v. 103, p. 504–511.

Goldblatt, P., and Manning, J.C., 2002, Plant diversity of the Cape Region of Southern Africa: Missouri Botanical Garden, Annals, v. 89, p. 281–302.

Hahn, A., Schefuß, E., Andò, S., Cawthra, H.C., Frenzel, P., Kugel, M., Meschner, S., Mollenhauer, G., and Zabel, M., 2017, Southern Hemisphere anticyclonic circulation drives oceanic and climatic conditions in late Holocene southernmost Africa: Climate of the Past, v. 13, p. 649–665.

Hall, M. 1984. Man's historical and traditional use of fire in southern Africa, *in* Booysen, P.deV., and Tainton, N.M., eds., Ecological Effects of Fire in South African Ecosystems: Heidelberg, Springer-Verlag, Ecological Studies, Analysis and Synthesis, v. 48, p. 39–52.

Hälbich, I.W., and Cornell, D.H., 1983. Metamorphic history of the Cape Fold Belt, *in* Söhnge, A.P.G., and Hälbich, I.W., eds., Geodynamics of the Cape Fold Belt: Geological Society of South Africa, Special Publication 12, p. 149–164.

Henshilwood, C.S., 1996, A revised chronology for the arrival of pastoralism in southernmost Africa: new evidence of sheep at ca. 2000 BP from BBC, South Africa: Antiquity, v. 70, p. 945–949.

Hogg, A.G., Hua, Q., Blackwell, P.G., Niu, M., Buck, C.E., Guilderson, T.P., Heaton, T.J., Palmer, J.G., Reimer, P.J., Reimer, R.W., Turney, C.S.M., and Zimmerman, S.R.H., 2013, SHCal13 Southern Hemisphere calibration, 0–50,000 years cal BP: Radiocarbon, v. 55, p. 1889–1903.

Hungr, O., 2000, Analysis of debris flow surges using the theory of uniformity: Earth Surface Processes and Landforms, v. 25, p. 483–495.

Jansen, J.D., and Brierley, G.J., 2004, Pool-fills: a window to palaeoflood history and response in bedrock-confined rivers: Sedimentology, v. 51, p. 901–925.

Karatson, D., Sztano, O., and Telbisz, T., 2002, Preferred clast orientation in volcaniclastic mass-flow deposits: application of a new photo-statistical method: Journal of Sedimentary Research, v. 72, p. 823–835.

Kemp, D.B., and Sexton, P.F., 2014, Timescale uncertainty of abrupt events in the geologic record arising from unsteady sedimentation: Geology, v. 42, p. 891–894.

Kraaij, T., and van Wilgen, B.W., 2014, Drivers, ecology, and management of fire in fynbos, *in* Allsopp, N., Colville, J.F., and Verboom, G.A., eds., Fynbos: Ecology Evolution and Conservation of a Megadiverse Region: Oxford, UK, Oxford University Press, p. 47–72.

Liu, G., and Cui, Z.,1999, Sedimentary macro-structures and forming mechanism of debris flow: Chinese Geographical Science, v. 9, p. 33–39.

Meyer, G.A., Wells, S.G., and Jull, A.J.T., 1995, Fire and alluvial chronology in Yellowstone National Park: climatic and intrinsic controls on Holocene geomorphic processes: Geological Society of America, Bulletin, v. 107, p. 1211–1230.

Miall, A.D., 1996, The Geology of Fluvial Deposits: Sedimentary Facies, Basin Analysis, and Petroleum Geology: Heidelberg, Springer-Verlag, p. 75–167.

Miall, A.D., 2014a, Updating uniformitarianism: stratigraphy as just a set of ‘frozen accidents’, *in* Smith, D.G., Bailey, R.J., Burgess, P.M., and Fraser, A.J., eds., 2014, Strata and Time: Probing the Gaps in Our Understanding: Geological Society of London, Special Publication 404, p. 11–36.

Miall, A.D., 2014b, The emptiness of the stratigraphic record: a preliminary evaluation of the missing time in the Mesaverde Group, Book Cliffs, Utah: Journal of Sedimentary Research, v. 84, p. 457–469.

Moll, E.J., McKenzie, B., and McLachlan, D., 1980, A possible explanation for the lack of trees in the fynbos, Cape Province, South Africa: Biological Conservation, v. 17, p. 221–228.

Moody, J.A., Shakesby, R.A., Robichaud, P.R., Cannon, S.H., and Martin, D.A., 2013, Current research issues related to post-wildfire runoff and erosion processes: Earth–Science Reviews, v. 122, p. 10–37.

Muir, R., Bordy, E.M., and Prevec, R., 2015, Lower Cretaceous deposit reveals first evidence of a post-wildfire debris flow in the Kirkwood Formation, Algoa Basin, Eastern Cape, South Africa: Cretaceous Research, v. 56, p. 161–179.

Nanson, G.C., 1986, Episodes of vertical accretion and catastrophic stripping – A model of disequilibrium floodplain development: Geological Society of America, Bulletin, v. 97, p. 1467–1475.

Nichols, G.J., Cripps, J.A., Collinson, M. E., and Scott, A.C., 2000, Experiments in waterlogging and sedimentology of charcoal: results and implications: Palaeogeography, Palaeoclimatology, Palaeoecology, v. 164, p. 43–56.

Nicholson, S.E., Nash, D.J., Chase, B.M., Grab, S.W., Shanahan, T.M., Verschuren, D., Asrat, A., Lezine, A.–M., and Umer, M., 2013, Temperature variability over Africa during the last, 2000 years: The Holocene, v. 23, p. 1085–1094.

PAGES 2k Consortium: Ahmed, M., Anchukaitis, K.J., Asrat, A., Borgaonkar, H.P., Braida, M., Buckley, B.M., Büntgen, U., Chase, B.M., Christie, D.A., Cook, E.R., Curran, M.A.J., Diaz, H.F., Esper, J., Fan, Z.–X., Gaire, N.P., Ge, Q., Gergis, J., González–Rouco, J.F., Goosse, H., Grab, S.W., Graham, N., Graham, R., Grosjean, M., Hanhijärvi, S.T., Kaufman, D.S., Kiefer, T., Kimura, K., Korhola, A.A., Krusic, P.J., Lara, A., Lézine, A.–M., Ljungqvist, F.C., Lorrey, A.M., Luterbacher, J., Masson–Delmotte, V., McCarroll, D., McConnell, J.R., McKay, N.P., Morales, M.S., Moy, A.D., Mulvaney, R., Mundo, I.A., Nakatsuka, T., Nash, D.J., Neukom, R., Nicholson, S.E., Oerter, H., Palmer, J.G., Phipps, S.J., Prieto, M.R., Rivera, A., Sano, M., Severi, M., Shanahan, T.M., Shao, X., Shi, F., Sigl, M., Smerdon, J.E., Solomina, O.N., Steig, E.J., Stenni, B., Thamban, M., Trouet, V., Turney, C.S.M., Umer, M., van Ommen, T., Verschuren, D., Viau, A.E., Villalba, R., Vinther, B.M., von Gunten, L., Wagner, S., Wahl, E.R., Wanner, H., Werner, J.P., White, J.W.C., Yasue, K., and Zorita, E., 2013, Continental-scale temperature variability during the past two millennia: Nature Geoscience, v. 6, p. 339–346.

POSTMA, G., 1984, Mass-flow conglomerates in a submarine canyon: Abrioja Fan-Delta, Pliocene, Southeast Spain, *in* Koster, E.H., and Steel, R.J., eds., Sedimentology of Gravels and Conglomerates: Canadian Society of Petroleum Geologists, Memoir 10, p. 237–256.

RIGGS, H.C., 1976, A simplified slope–area method for estimating flood discharges in natural channels: U.S. Geological Survey, Journal of Research, v. 4, p. 285–291.

RYAN, S.E., DWIRE, K.A., AND DIXON, M.K., 2011, Impacts of wildfire on runoff and sediment loads at Little Granite Creek, western Wyoming: Geomorphology, v. 129, p. 113–130.

Sadr K., 2015, Livestock first reached southern Africa in two separate events. PLoS ONE 10(8): e0134215. https://doi.org/10.1371/journal.pone.0134215

Schapera, I., 1930. The Khoisan Peoples of South Africa: London, Routledge & Kegan. 450 p.

Scharf, T.E., Codilean, A.T., de Wit, M., Jansen, J.D., and Kubik, P.W., 2013, Strong rocks sustain ancient postorogenic topography in southern Africa: Geology, v. 41, p. 331–334.

Scott, D.F., 1993, The hydrological effects of fire in South African mountain catchments: Journal of Hydrology, v. 150, p. 409–432.

Sealy, J.C., and Yates, R., 1994, The chronology of the introduction of pastoralism to the Cape, South Africa: Antiquity, v. 68, p. 58–67.

Seydack, A.H.W., Bekker, S.J., and Marshall, A.H., 2007, Shrubland fire regime scenarios in the Swartberg Mountain Range, South Africa: implications for fire management: International Journal of Wildland Fire, v. 16, p. 81–95.

Shultz, A.W., 1984, Subaerial debris-flow deposition in the Upper Paleozoic Cutler Formation, Western Colorado: Journal of Sedimentary Petrology, v. 54, p. 759–772.

Smith, D.G., Hubbard, S.M., Lavigne, J.R., Leckie, D.A., and Fustic, M., 2011, Stratigraphy of the counter-point-bar and eddy-accretion deposits in low-energy meander belts of the Peace–Athabasca Delta, Northeast Alberta, Canada, *in* Davidson, S., Leleu, S., and North, C.P., eds., From River to rock Record; the Preservation of Fluvial Sediments and Their Subsequent Interpretation: SEPM (Society for Sedimentary Geology), Special Publication 97, p. 143–152.

Smith, D.G., Bailey, R.J., Burgess, P.M., and Fraser, A.J., 2015, Strata and Time; Probing the Gaps in Our Understanding: Geological Society of London, Special Publication 404, p. 1–10.

Sohn, Y.K., Rhee, C.W., and Kim, B.C., 1999, Debris flow and hyperconcentrated flood–flow deposits in an alluvial fan, northwestern part of the Cretaceous Yongdong Basin, Central Korea: The Journal of Geology, v. 107, p. 111–132.

Sohn, Y.K., Choe, M.Y., and Jo, H.R., 2002, Transition from debris flow to hyperconcentrated flow in a submarine channel (the Cretaceous Cerro Toro Formation, southern Chile): Terra Nova, v. 14, p. 405–415.

Soler, M., and Sala, M., 1992, Effects of fire and of clearing in a Mediterranean *Quercus ilex* woodland: An experimental approach: Catena, v. 19, p. 321–332.

Stear, W.M., 1985, Comparison of the bedform distribution and dynamics of modern and ancient sandy ephemeral flood deposits in the southwestern Karoo region, South Africa: Sedimentary Geology, v. 45, p. 209–230.

Takahashi, T., 1991, Debris flow: International Association for Hydro-Environment Engineering and Research (IAHR), Monograph Series: Rotterdam, Balkema, 165 p.

Van Bladeren, D., Zawada, P.K., and Mahlangu, D., 2007, Statistical based regional flood frequency estimation study for South Africa using systematic, historical and palaeoflood data: Pretoria, Water Research Commission, Report 1260-1-07, p. 1–252. Available at http://www.wrc.org.za

WHITLOCK, C., AND LARSEN, C., 2002, Charcoal as a fire proxy, *in* SMOL, J.P., BIRKS, H.J.B., and LAST, W.M., eds., Tracking Environmental Change Using Lake Sediments: Dordrecht, The Netherlands, Kluwer Academic Publishers, p. 75–97.

WILLIAMS, G.P, 1978, Bankfull discharge of rivers: Water Resources Research, v. 14, p. 1141–1154.

WILLIAMS, G.P., AND COSTA, J.E., 1988, Geomorphic measurements after a flood, *in* Baker, V.C., Kochel, R.C., and Patton, P.C. eds., Flood Geomorphology: New York, John Wiley & Sons, p. 65–76.

ZAWADA, P.K., 1994, Palaeoflood hydrology of the Buffels River, Laingsburg: South African Journal of Geology, v. 97, p. 21–32.

Figure captions

Fig. 1. Geological map and the key geomorphological features of the study area located in upper Huis River directly SE of Barrydale (Western Cape, South Africa) in the SW Cape Fold Belt. Close-up aerial photograph illustrates the key study sites. The Holocene sediments are best preserved at the confluence (GPS coordinate: 33° 55' 5.03" S; 20° 45' 2.42" E) as well as in a small cave and along three meander bends of the canyon (see person for scale). Map sources: Google Earth (2013), own oen mapping. and CGS (1997).

Fig. 2. Summary of sedimentary facies of the Holocene sediments in the upper Huis River.

Fig. 3. Schematic geological maps indicating the spatial distributions of the five facies associations (FAs) in the upper Huis River. Gray shading approximates the topographic contours; not to scale. The present-day channels of the upper Huis River and its tributary are schematically demarcated in blue; see caption of Figure 1 for the GPS coordinate of the confluence point.

Fig. 4. **A)** Schematic summary of the stratigraphic relationships between Facies Associations A to E (not to scale). The base of the cave sediments (FA-C) is 1.06 m below the upper surface of FA-B and ~ 11 m above the present river channel. **B)** Stratigraphic relationships between FA-A, FA-B, and FA-D at the confluence. Arrows mark the FAs, and the shades of colors indicate the facies contained in them: red shades for the facies in FA-A, yellow shades for the facies in FA-B, and green shades for the facies in FA-D.

Fig. 5. Representative sedimentary features of FA-A and FA-B. **A)** In FA-A, rare rounded clasts in facies Gcm. Scale bar: 20 cm **B)** In FA-A, transitioning from facies Gcm, through matrix-supported, normally graded gravel (facies Gmg) to facies Gmm. Scale bar: 35 cm. **C)** Horizontal large clast and subvertical smaller clasts in facies Gmm of FA-B. **D)** In FA-B,

zones of relatively high and low abundance of clasts in facies Gmm. Note the variation in clast size. Scale bar: 70 cm. **E)** In facies Gms of FA-B, stratification is shown both by 0.5-10 mm diameter clast stringers and flat charcoal fragments (inset shows close-up of the marked area). Upward-pointing arrow for normal grading; double arrow for inverse-to-normal grading. **F)** Facies Gms often occurs in the upper part of FA-B. Note the localized clast-supported gravel patches.

Fig. 6. Representative sedimentary features of FA-B, FA-C, and FA-D. **A)** In FA-B, the "linear circling" feature, the lens of sediment to the left of the large boulder (A – photo and A' – line drawing) represents the transition from facies Gmm to facies Gms. **B)** In FA-B, a lens of facies SGmm in a thick bed of facies Gmm. **C)** Outcrop of planar laminated organic detritus (facies Ol) in the cave (FA-C). Note the large, very angular quartzite clast that has fallen into facies Ol from the cave walls (roof). **D)** Alternating layers of matrix-supported, inversely graded sandy gravels (facies SGmi) and facies Sm overlying facies Gcm in FA-D. Beds marked in D' are based on the high-resolution field observations of subtle facies changes that are only faintly visible in D.

Fig. 7. Model for the emplacement of FA-B (not to scale). **A)** Precursory surge enters confluence, erodes FA-A (red), and deposits initial FA-B facies. **B)** Main debris flow freezes as front loses momentum. **C)** Secondary surges cause rear parts of debris flow to override the frozen front, and deposition takes place until critical angle is reached. **D)** Hyperconcentrated and fluvial flow override existing deposits (light green and blue).

Fig. 8. Schematic depositional model for FA-C (flow of the Huis River is from left to right) in the cave site. **A)** Peak discharge following deposition of FA-B created erosional eddy current that cleared the sediments that were deposited there previously. **B)** Eddy current trapped suspended sediments in the cave, allowing the accumulation of coarse sands (facies

Smo) at base of vortex and trapping a floating charcoal-rich mat on the surface. **C)** As flow level decreased, suspended fines were rapidly deposited together with the now waterlogged charcoal mat (Om). **D)** Events B to C may have been repeated in subsequent peak discharges (of the same or different flood events). **E)** Pools left being in the cave provided the quiet-water setting where small charcoal fragments and the other fine-grained deposits settled out from suspension (facies Ol) (**F**).

Fig. 9. Representative sedimentary features of FA-D. **A)** A lens of clast-supported massive gravel (facies Gcm). Overlying and underlying sediment is massive sand facies (Sm). Note the imbrication from left to right in the tabular clasts (marked with dashed line). **B)** Subrounded rip-up clast of local provenance found in facies Gcm (clast-supported massive gravel of FA-D). This 12.5-cm-long rip-up clast consists of matrix-supported small-pebble breccia and was found deeply embedded in the southern outcrops of facies Gcm. Tape-measure markings are in inches (= 2.54 cm). **C)** Example of sharply defined layer of facies SGmi between two layers of massive sand (facies Sm). Note the inverse grading in facies SGmi. **D)** Anomalously large 12 cm and 5 cm clasts in an otherwise standard layer of facies SGmi in FA-D. Note that outcrop was covered in a thin plaster of modern mud slurry that obscures some of the key features of facies SGmi in this picture. Scale bar: 20 cm. **E)** A lens of clast-supported gravel (facies Gcm) in a matrix-supported, inversely graded sandy gravel (facies SGmi) bed, overlain and underlain by massive sand (facies Sm). Material in the lower right corner is not *in situ*. **F)** Typical interbedding of the massive sand (facies Sm) and matrix-supported, inversely graded sandy gravel (facies SGmi) of FA-D. Note the erosional relationship between the lower surface of the facies SGmi layers and the facies Sm. Scale bar: 50 cm.

Fig. 10. Representative sedimentary features of FA-E. **A)** Plan view of a veneer of facies Gcb that served as a pebble armor, hindering the erosion of underlying sediments. Scale bar: 50 cm. **B)** Clast-supported imbricated gravel (facies Gcb) lenses in vertically stacked sediment of facies Gmm and Sm. Note the imbrication of the tabular clasts near the tape. Scale bar: 72 cm. **C)** View of Boulder Bar 2 in a bend of the bedrock-confined river bed. Scale bar: double-arrows each marking 12 m vertically (apparent size difference is due to the aerial perspective). Note the very sharp, horizontal line on the canyon wall, which marks a distinct change in plant density and the upper limit of FA-B. Below the line, the canyon wall was stripped in the last, abrading extreme paleoflood (hence the white bedrock is more exposed and only small, isolated patches of FA-B are preserved in this part of the bedrock canyon). **D)** Massive, charcoal-rich sand (facies Sm) overlain by a clast-supported imbricated gravel veneer (facies Gcb) and underlain by facies Gcb in Boulder Bar 2. **E)** Imbrication of the tabular, subrounded to subangular clasts (facies Gcb) in the Boulder Bar 2. Person for scale. **F)** Close-up view of crescentic attrition (“chatter”) marks on the surface of a rounded quartzite boulder indicating bedload transport of the clasts by extremely powerful currents.

Fig. 11. Sedimentological history of the Holocene sediments in the upper Huis River. **Event 1:** Wildfire takes place in the upper Huis River catchment. **Event 2:** Sediments are accumulating and may be slowing mobilizing in mass movements in the burned catchment. **Event 3**: Peak discharge event occurs, colluvium is mobilized. Immature debris flow from tributary reaches the confluence, depositing FA-A. **Event 4:** Precursory surge of the main debris-flow enters the confluence area, partially eroding FA-A. **Event 5**: Main debris flow surge is immobilized at the confluence mouth, depositing FA-B. Internal stress creates chaotic fabrics. **Event 6**: The tail zone begins to override the frozen main debris flow. **Event 7**: Overriding debris flow passes the frozen debris-flow front. Further deposition of FA-B takes place in the confluence area. **Event 8**: The hyperconcentrated and fluvial parts of the sediment-gravity-flow tail zone override the

debris-flow sediments, forming the facies SGmg and Sm at the top of FA-B. Eddy currents created by this flow cause sediment erosion in the cave. **Event 9**: Flood recedes and initial FA-C is deposited in the cave. **Event 10**: Sustained streamflow resumes. Upstream FA-B sediments are eroded. Redeposited sediment causes channel aggradation, depositing initial FA-E. **Event 11**: A smaller flood occurs in the upper Huis River catchment (possibly following another wildfire). Channel incision into the frozen-debris-flow front causes gravity winnowing. Eddy currents remobilize some cave sediments. **Event 12**: Winnowed sediments are remobilized and an immature debris flow forms at the confluence, depositing a package of FA-D. **Event 13**: Flood recedes and slackwater deposits (facies Ol) of FA-D are deposited at the confluence. Another unit of FA-C is deposited in the cave. **Event 14**: Events laid out in 11-13 are repeated, and gravel armoring (FA-E) occurs. **Event 15**: Further channel incision in at least two extreme paleofloods carve out the present-day topography and deposits the two major boulder bars at 894 ± 37 BP and at 653 ± 35 BP.

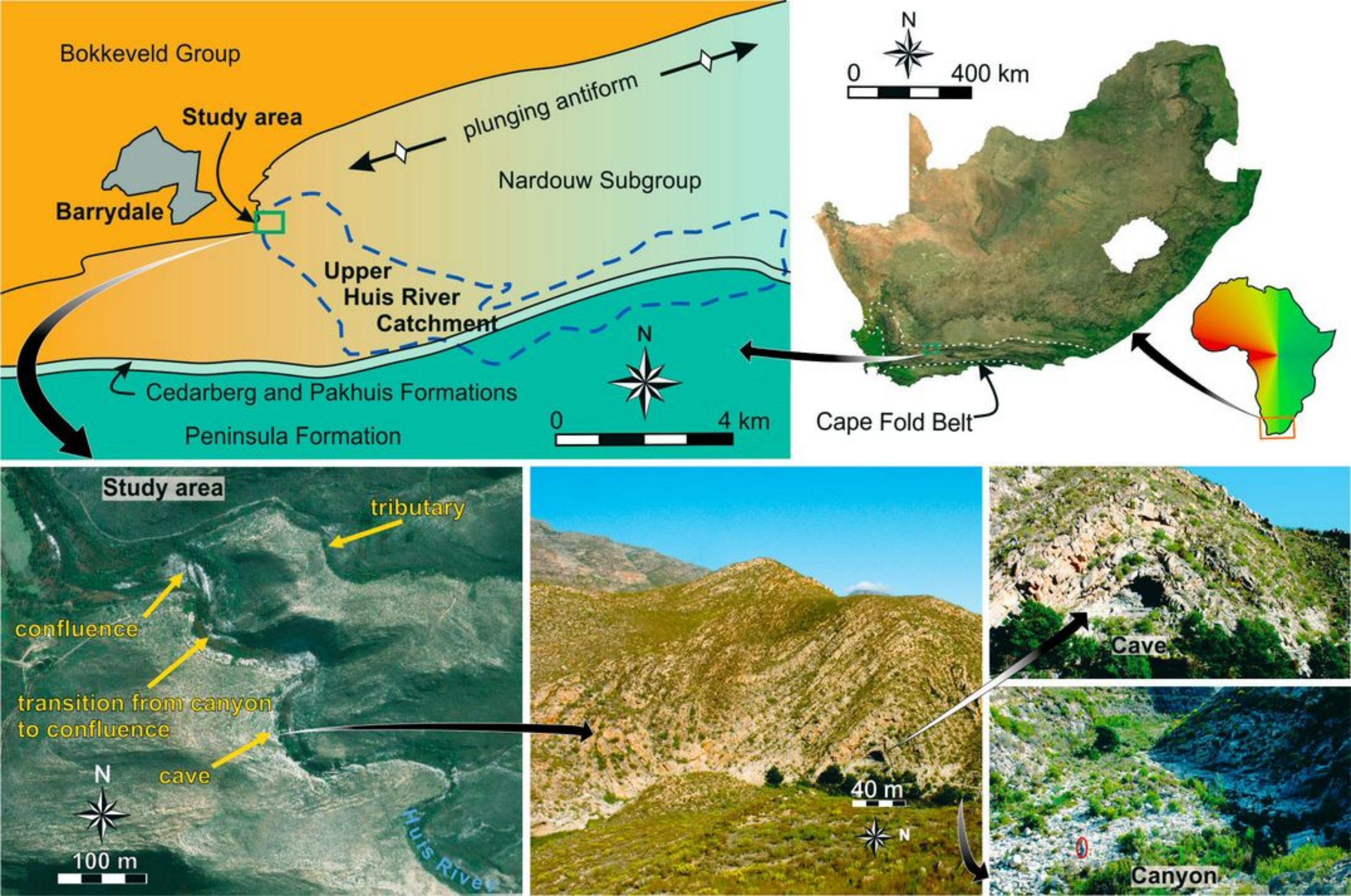
Bokkeveld Group
plunging antiform
Study area
Barrydale
Nardouw Subgroup
Upper
Huis River
Catchment
Cedarberg and Pakhuis Formations
Peninsula Formation
N
0
4 km
0
400 km
Cape Fold Belt
Study area
tributary
confluence
transition from canyon
to confluence
cave
100 m
Huis River
40 m
N
Cave
Canyon

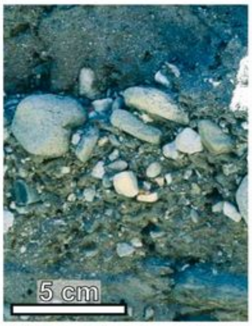

Gcb
Clast-supported imbricated gravel
Dominant in FA-E
Streamflow process

Gcm
Clast-supported massive gravel
Dominant in FA-A, uncommon in FA-D
Psuedoplastic debris flow

Gmg
Matrix-supported normally graded gravel
Common in FA-A
Transition from low- to high-matrix-strength debris flow

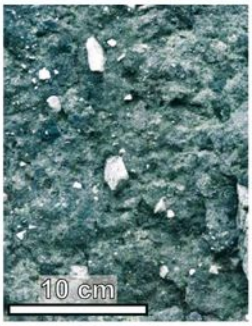

Gmm
Matrix-supported massive gravel
Common FA-A and FA-B
High-strength, plastic debris flow

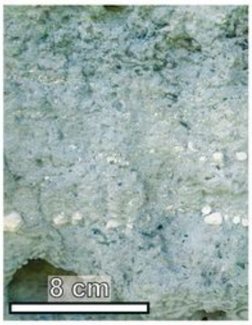

Gms
Matrix-supported stratified gravel
Exclusive to FA-B
Abundant charcoal fragments
Transitional debris flow

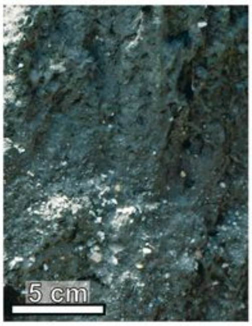

Sgmg
Matrix-supported normally graded sandy gravel
Exclusive to FA-B
Low-strength, psuedoplastic debris flow

Sgmi
Matrix-supported inversely graded sandy gravel
Common in FA-D
Sediment gravity flow
Abundant charcoal fragments

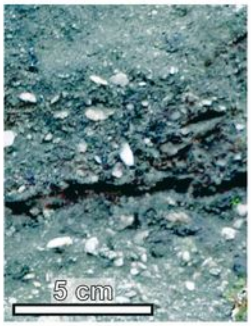

Sgmm
Matrix-supported massive sandy gravel
Exclusive to confluence FA-B
High-strength, plastic debris flow

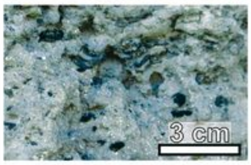

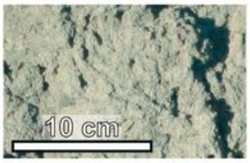

Sm
Massive sand, can be very rich in charcoal fragments
Common in FA-B, FA-D and FA-E
Sediment gravity flow or postdepositional modification

Smo
Massive open framework sand
Exclusive to, but rare in FA-C
Eddy deposit

Ol
Planar laminated organic detritus
Common in FA-C, rare in FA-D
Deposition from suspension

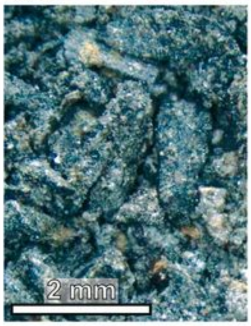

Om
Massive organic detritus
Dominant in FA-C
Deposition of floating mat from suspension

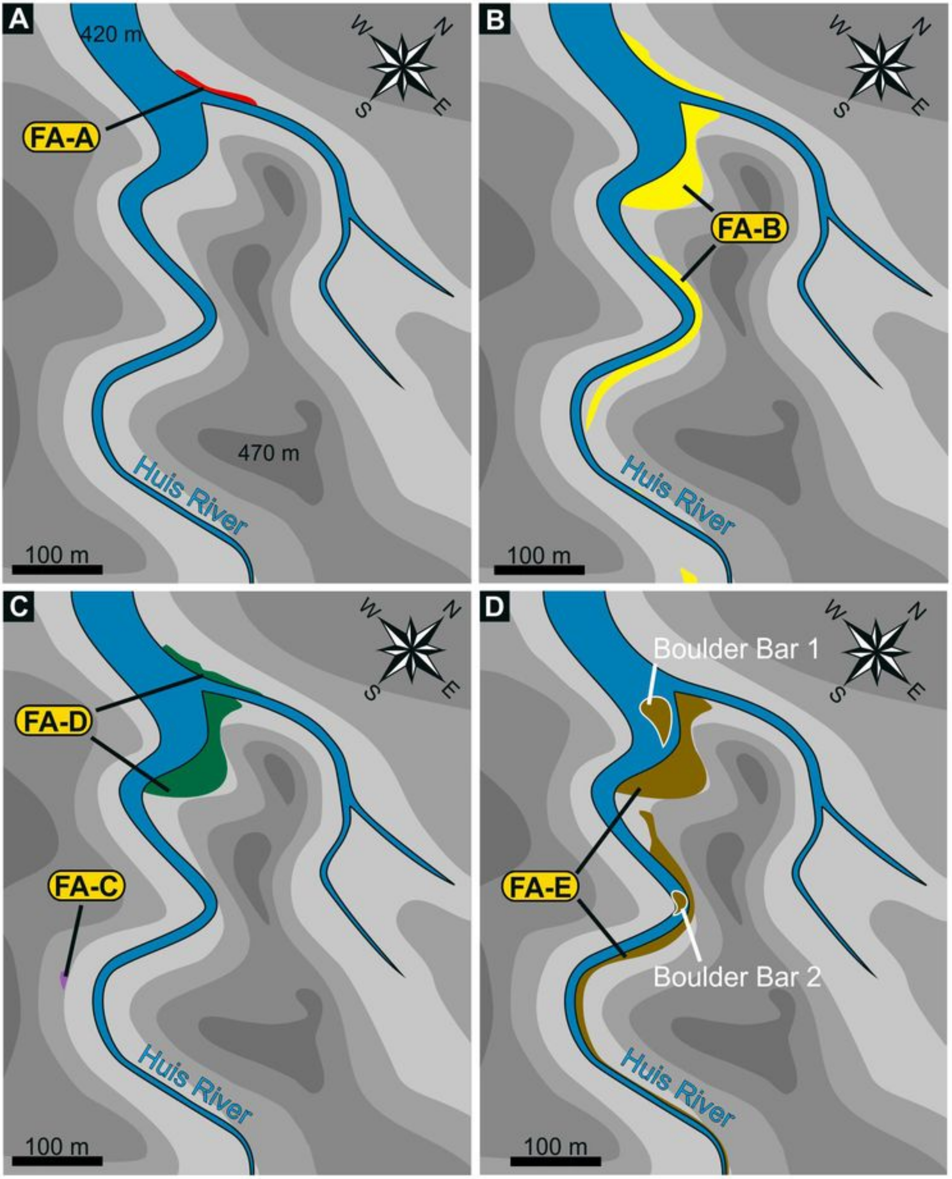
A
420 m
FA-A
470 m
Huis River
100 m
B
FA-B
Huis River
100 m
C
FA-D
FA-C
Huis River
100 m
D
Boulder Bar 1
FA-E
Boulder Bar 2
Huis River
100 m
W
N
S
E

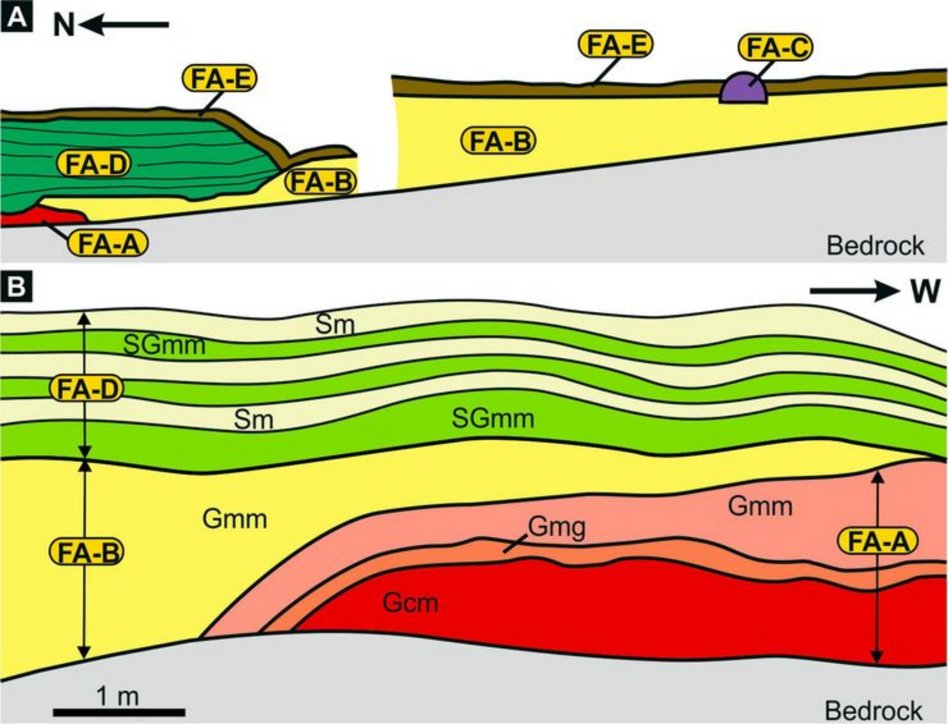

A
N
FA-E
FA-E
FA-C
FA-D
FA-B
FA-B
FA-A
Bedrock
B
W
Sm
SGmm
FA-D
Sm
SGmm
Gmm
Gmm
Gmg
FA-B
FA-A
Gcm
1 m
Bedrock

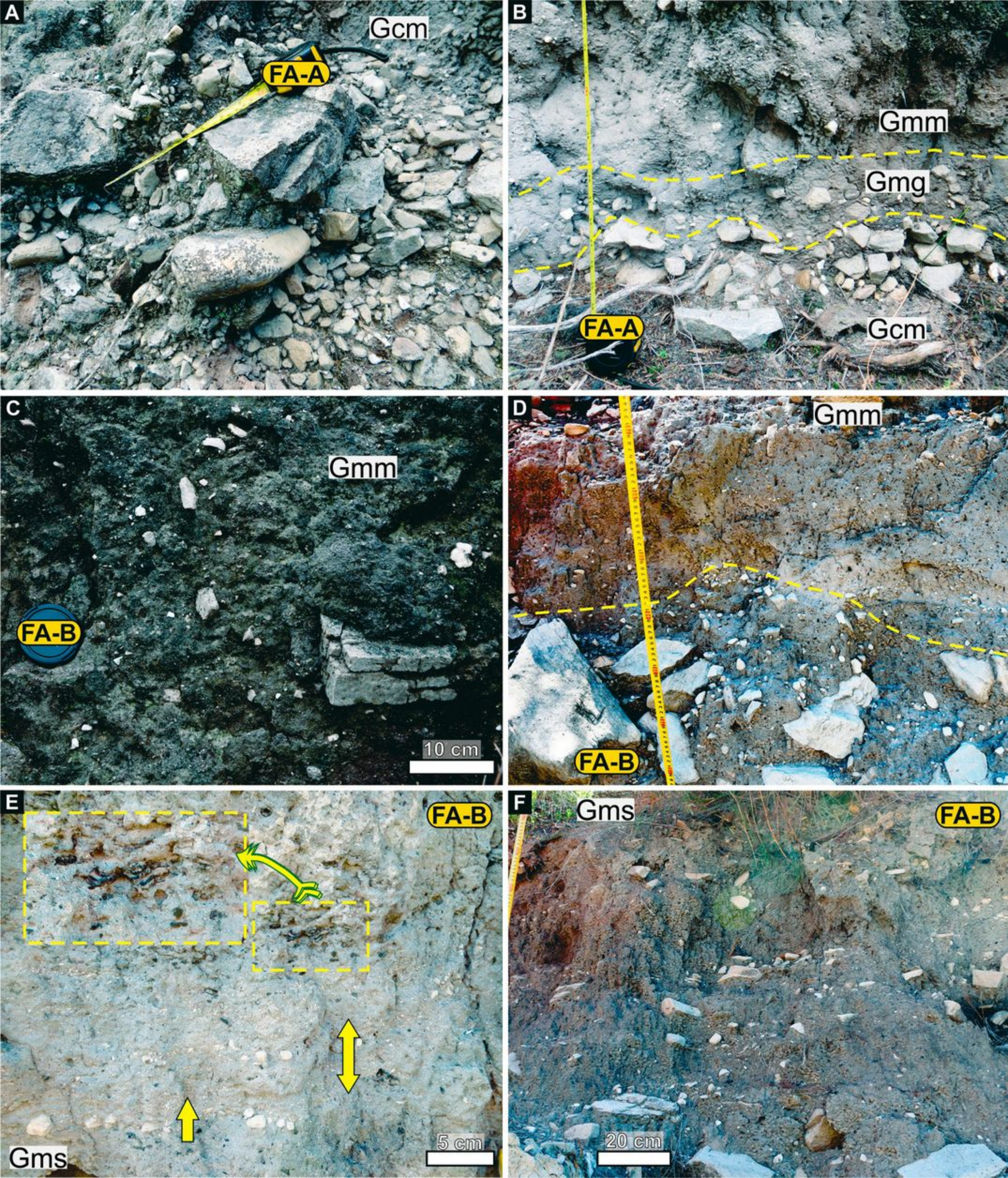
A
Gcm
FA-A
B
Gmm
Gmg
Gcm
FA-A
C
Gmm
FA-B
10 cm
D
Gmm
FA-B
E
FA-B
Gms
5 cm
F
Gms
FA-B
20 cm

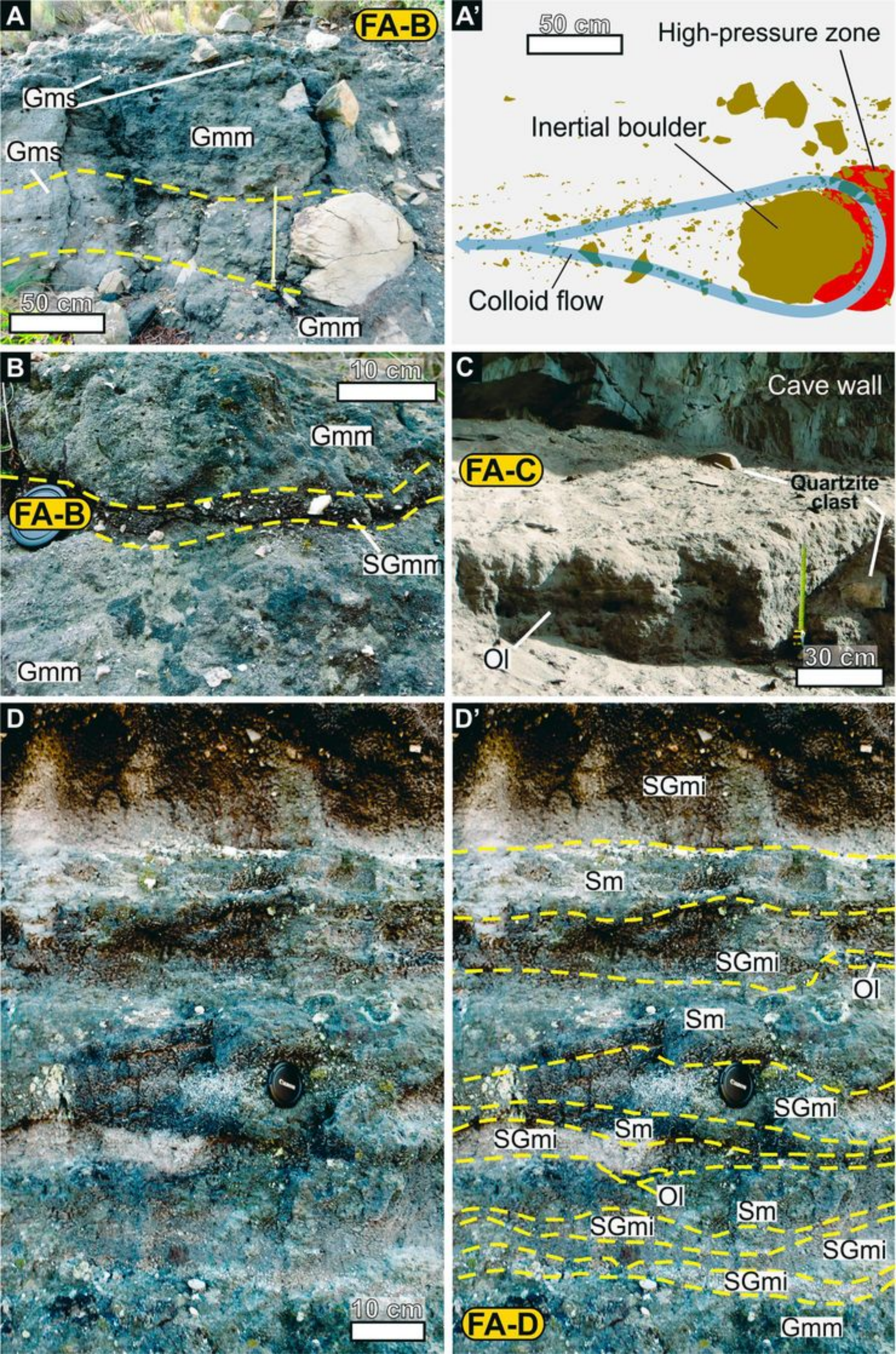
A
FA-B
Gms
Gms
Gmm
50 cm
Gmm
A'
50 cm
High-pressure zone
Inertial boulder
Colloid flow
B
10 cm
Gmm
FA-B
SGmm
Gmm
C
Cave wall
FA-C
Quartzite clast
Ol
30 cm
D
10 cm
D'
SGmi
Sm
SGmi
Ol
Sm
SGmi
SGmi
Sm
Ol
Sm
SGmi
SGmi
SGmi
FA-D
Gmm

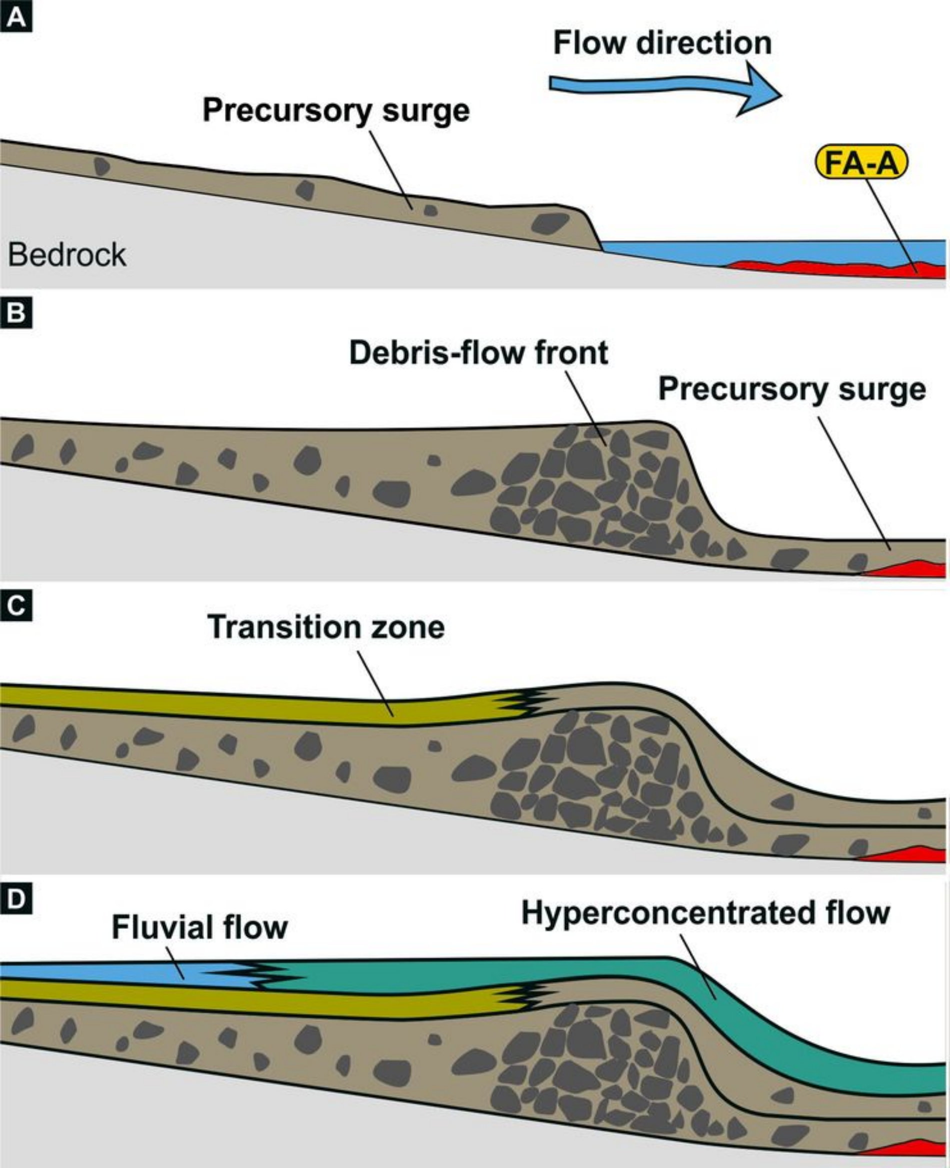
A
Flow direction
Precursory surge
FA-A
Bedrock
B
Debris-flow front
Precursory surge
C
Transition zone
D
Fluvial flow
Hyperconcentrated flow

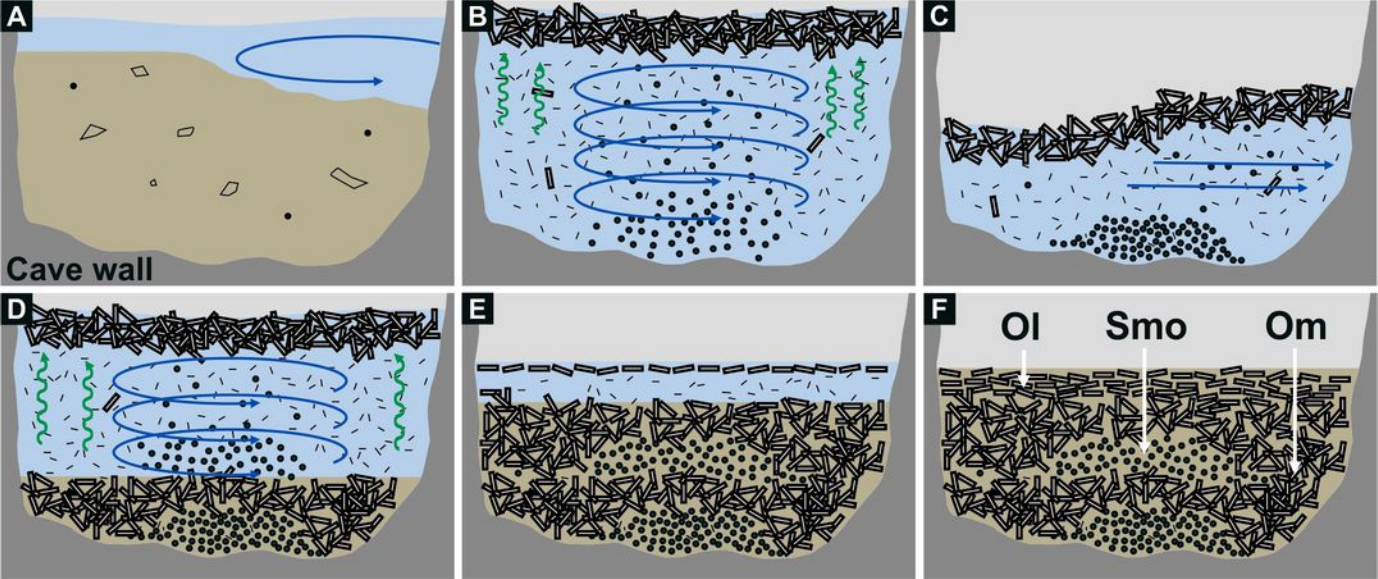
A
Cave wall
B
C
D
E
F
Ol
Smo
Om

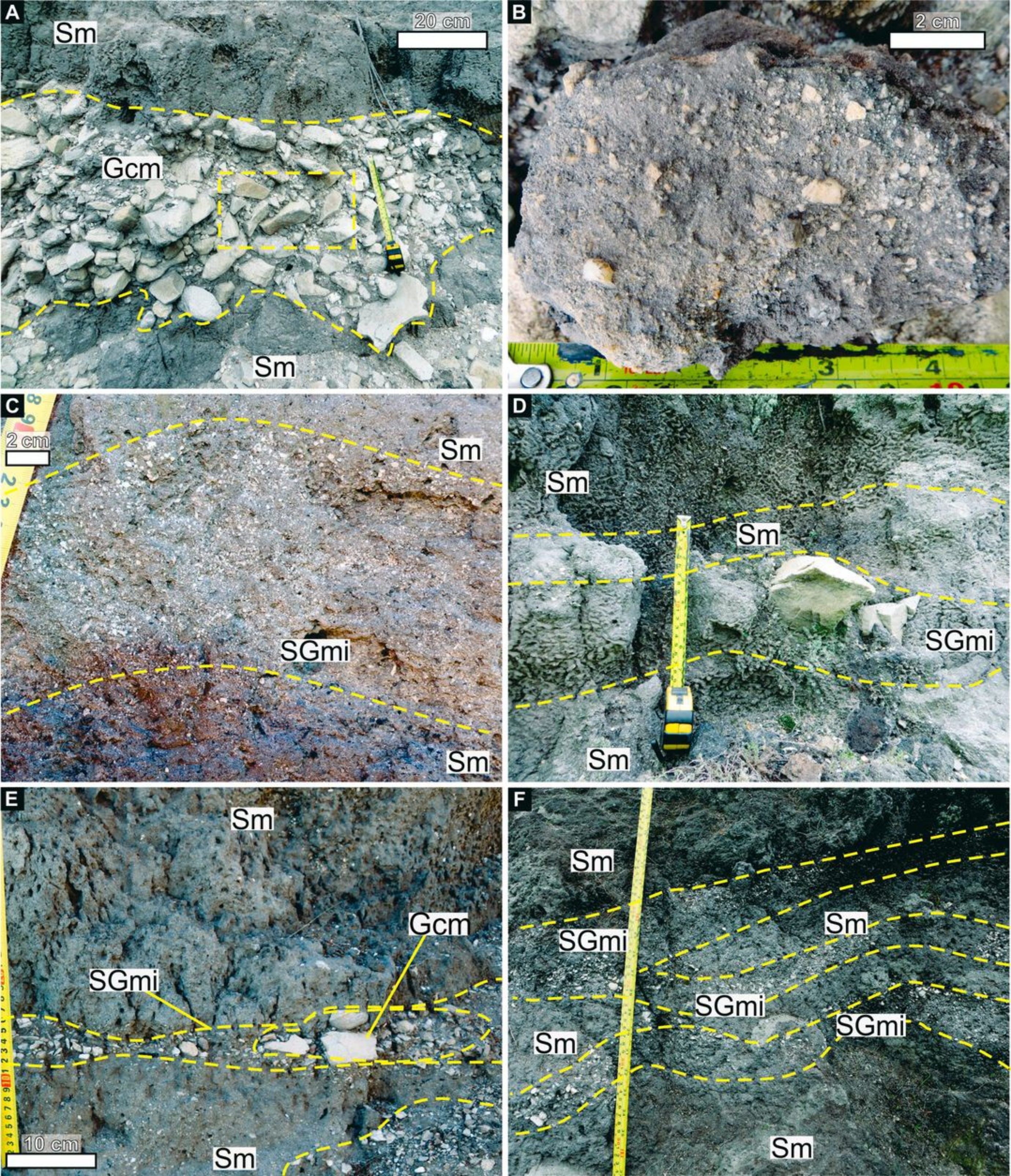

A
Sm
20 cm
Gcm
Sm
B
2 cm
C
2 cm
Sm
SGmi
Sm
D
Sm
Sm
SGmi
Sm
E
Sm
SGmi
Gcm
10 cm
Sm
F
Sm
SGmi
Sm
SGmi
SGmi
Sm
Sm

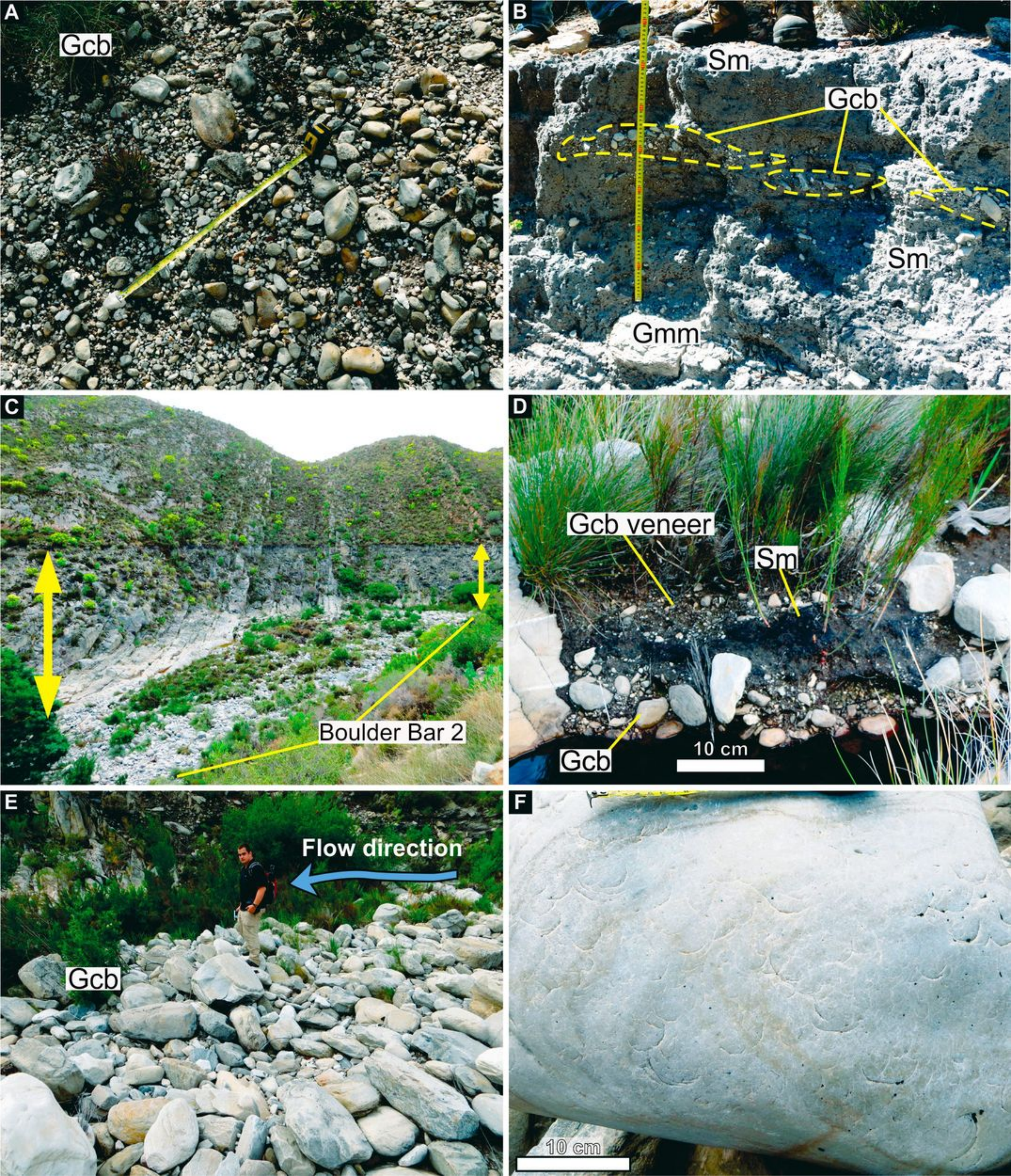
A
Gcb
B
Sm
Gcb
Sm
Gmm
C
Boulder Bar 2
D
Gcb veneer
Sm
Gcb
10 cm
E
Flow direction
Gcb
F
10 cm

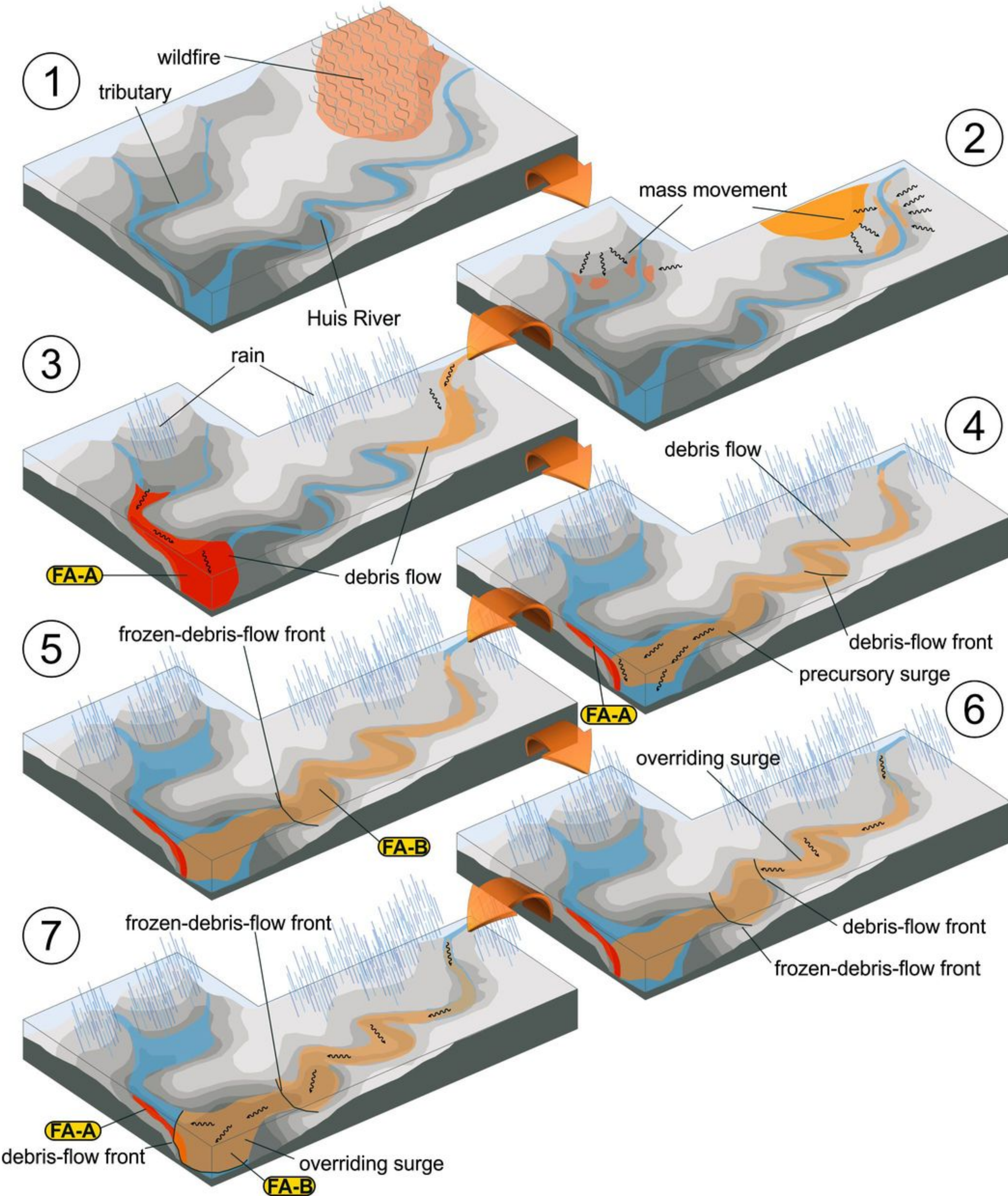

1
wildfire
tributary
Huis River
2
mass movement
3
rain
debris flow
FA-A
4
debris flow
debris-flow front
precursory surge
FA-A
5
frozen-debris-flow front
FA-B
6
overriding surge
debris-flow front
frozen-debris-flow front
7
frozen-debris-flow front
FA-A
debris-flow front
overriding surge
FA-B

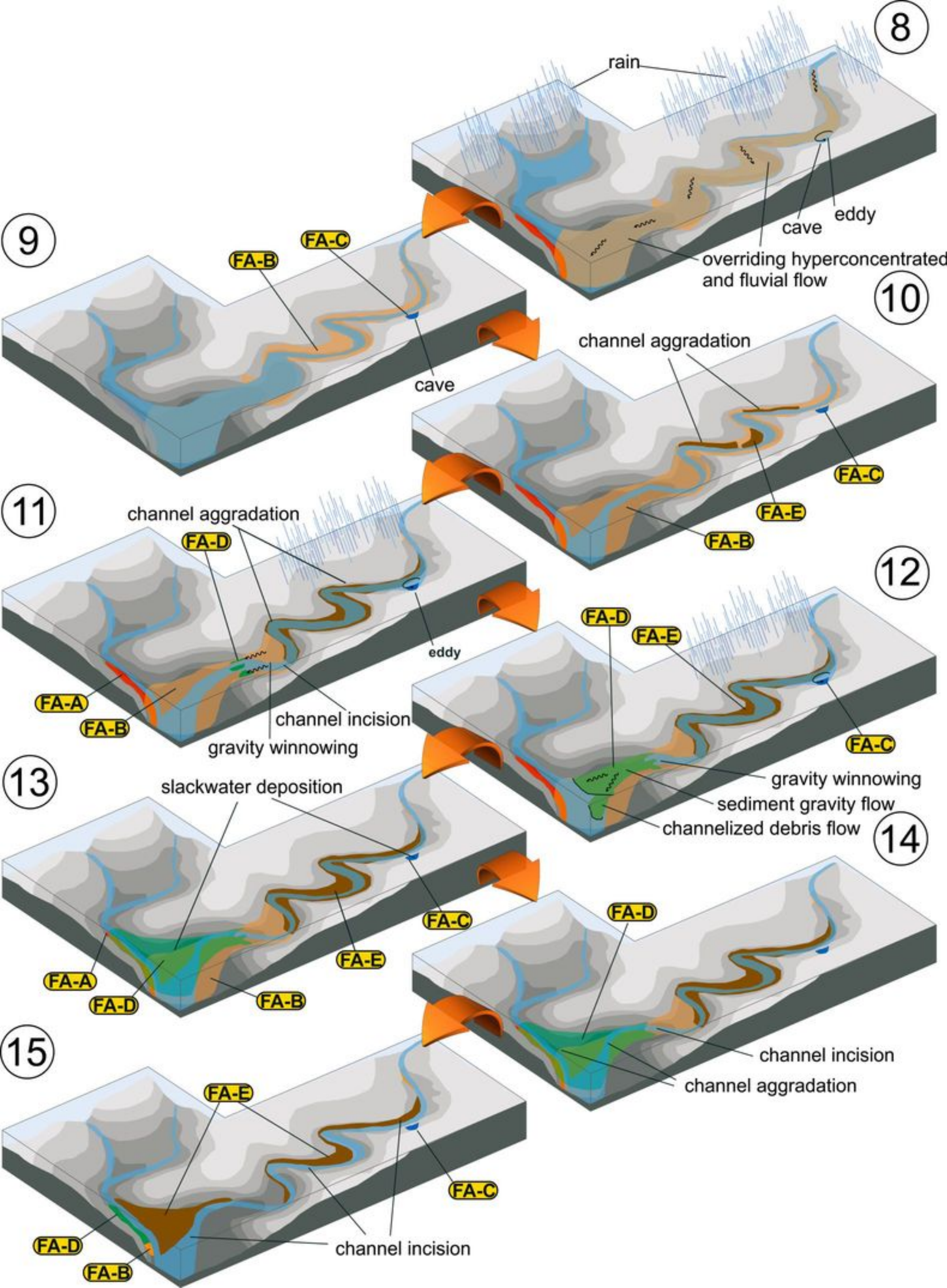

8
rain
eddy
cave
overriding hyperconcentrated and fluvial flow
9
FA-B
FA-C
cave
10
channel aggradation
FA-C
FA-E
FA-B
11
channel aggradation
FA-D
eddy
FA-A
FA-B
channel incision
gravity winnowing
12
FA-D
FA-E
FA-C
gravity winnowing
sediment gravity flow
channelized debris flow
13
slackwater deposition
FA-C
FA-E
FA-A
FA-D
FA-B
14
FA-D
channel incision
channel aggradation
15
FA-E
FA-C
FA-D
FA-B
channel incision

Table 1. Summary of the facies associations of Holocene sediments in the upper Huis River, including the internal facies compositions (see Fig. 2), sediment transport processes, and interpretations (see text for details). Note that the radiocarbon ages of the dated facies associations are also shown.

Facies Association	Characteristic Facies	Sediment transport process	Interpretation	Calibrated radiocarbon ages	Age BP	SUERC #
A	Gcm, Gmm, Gmg	High-viscosity flows in mass movement	Pseudoplastic-debris-flow deposits			
B	Gmm, Gms, SGmg, SGmm, Sm	Intermediate-viscosity flows in mass movement	Transitional-debris-flow deposits	353-294 cal BC and 231-58 cal BC	2165 ± 35 BP	SUERC-35169
C	Smo, Ol, Om	Low-viscosity flows in mass movement, eddy currents	Slackwater deposits in cave	390-573 cal AD	1628 ± 37 BP	SUERC-36432
D	Gcm, SGmi, Sm, Ol	Traction currents, low-viscosity flows	Flash-flood deposits			
E	Gcb*, Sm, Gmm *including the boulder bars at the confluence (BB1) and in the canyon (BB2)	Fast-flowing sediment-laden waters	River-flow deposits	(BB1) 1051-1080 cal AD and 1145-1271 cal AD	(BB1) 894 ± 37 BP	(BB1) SUERC-36431
				(BB2) 1297-1404 cal AD	(BB2) 653 ± 35 BP	(BB2) SUERC-35166

Table 2. Rough estimates of discharge (*Q*) (in m^3/s) for the paleoflood events in the bedrock canyon of the upper Huis River based on calculation suggested in Riggs (1976), Williams (1978), and Costa (1983). The latter estimates the mean flow velocity (*V*) using a formula that requires the average length of the intermediate axis of the five largest boulders (*d*), which is ~ 1 m in the boulder bar near cross sections 2 and 3. See text for details.

	Cross section 1	**Cross section 2**	**Cross section 3**	**Average**
A = cross-sectional flow area (m^2)	275	439	455	390
S = channel slope (m/m)	0.064	0.064	0.064	0.064
Q = 3.39 * *A*^1.30 * *S*^0.32 (m^3/s) (Riggs, 1976)	2086	3832	4014	3285
Q = 4.0 * *A*^1.21 * *S*^0.32 (m^3/s) (Williams, 1978)	1657	2919	3048	2529
V = 0.18 * *d*^0.487 (m/s)				5.2
Q = *V* * *A* (m^3/s) (Costa, 1983)	No bar here	2284	2367	2326